UBR5 is co-amplified with MYC in breast tumors and encodes an ubiquitin ligase that limits MYC-dependent apoptosis

Xi Qiao[1,2,3], Ying Liu[4,5*], Maria Llamazares Prada[6*#], Aravind K. Mohan[7], Abhishekh Gupta[8], Alok Jaiswal[8], Mukund Sharma[1,2,3], Joni Merisaari[1,2,3], Heidi M. Haikala[9], Kati Talvinen[2], Laxman Yetukuri[1,8], Joanna W. Pylvänäinen[10], Juha Klefström[9], Pauliina Kronqvist[2], Annika Meinander[7], Tero Aittokallio[8,11], Ville Hietakangas[4,5], Martin Eilers[6], and Jukka Westermarck[1,2&]

[1]Turku Bioscience Centre, University of Turku and Åbo Akademi University, Turku, Finland

[2] Institute of Biomedicine, University of Turku, Turku, Finland

[3] TuDMM Doctoral Programme, University of Turku, Turku, Finland

[4] Faculty of Biological and Environmental Sciences, University of Helsinki

[5] Institute of Biotechnology, University of Helsinki

[6] Theodor Boveri Institute and Comprehensive Cancer Center, Mainfranken, Biocenter, University of Würzburg, Würzburg, Germany

[7] Faculty of Science and Engineering, Cell Biology, Åbo Akademi University, Turku, Finland

[8]Institute for Molecular Medicine Finland (FIMM), University of Helsinki, Helsinki, FI-00014 Finland

[9] Research Programs Unit /Translational Cancer Medicine & HiLIFE, University of Helsinki, Helsinki, Finland

[10] Turku BioImaging, University of Turku and Åbo Akademi University, Turku, Finland

[11] Department of Mathematics and Statistics, University of Turku, Turku, FI-20014, Finland

[*] These authors contributed equally

[#] Current address: BioMed X Innovation Center, Heidelberg, Germany

Running title: Ubiquitin ligase UBR5 controls MYC in development and cancer

Keywords: Irinotecan, Topotecan, Taxol, MYCN, TNBC

The authors declare no potential conflicts of interest

[&] To whom the correspondence should be addressed: Jukka Westermarck, Turku Bioscience Centre, Tykistökatu 6A, 20520 Turku, FINLAND; Phone: +358-29-450 2880; e-mail: jukka.westermarck@bioscience.fi

Abstract

For maximal oncogenic activity, cellular MYC protein levels need to be tightly controlled so that they do not induce apoptosis. Here, we show how ubiquitin ligase UBR5 functions as a molecular rheostat to prevent excess accumulation of MYC protein. UBR5 ubiquitinates MYC, and its effects on MYC protein stability are independent of FBXW7. Silencing of endogenous UBR5 induced MYC protein expression and regulated MYC target genes. Consistent with the tumor suppressor function of UBR5 (Hyd) in Drosophila, Hyd suppressed dMyc-dependent overgrowth of wing imaginal discs. In contrast, in cancer cells UBR5 suppressed MYC-dependent priming to therapy-induced apoptosis. Of direct cancer relevance, MYC and UBR5 genes were co-amplified in MYC-driven human cancers. Functionally, UBR5 suppressed MYC-mediated apoptosis in p53-mutant breast cancer cells with UBR5/MYC co-amplification. Further, single-cell immunofluorescence analysis demonstrated reciprocal expression of UBR5 and MYC in human basal-type breast cancer tissues. In summary, UBR5 is a novel MYC ubiquitin ligase and an endogenous rheostat for MYC activity. In MYC amplified, and p53-mutant breast cancer cells, UBR5 has an important role in suppressing MYC-mediated apoptosis priming and in protection from drug-induced apoptosis.

Significance:

Findings identify UBR5 as a novel MYC regulator, the inactivation of which could be very important for understanding of MYC dysregulation on cancer cells.

Introduction

Emerging notion of overall poor concordance between gene amplifications and corresponding protein expression levels in cancer (1) highlights the need for better understanding of how protein expression levels are regulated at post-translational levels. The transcription factor MYC regulates numerous physiological and pathological processes. Critically, distinct protein expression levels dictate MYC's biological output *in vitro* and *in vivo* (2-5). MYC protein levels are tightly regulated post-translationally by phosphorylation, and by ubiquitin-mediated degradation (6-10). Especially in cancers, MYC is a classic example of an oncoprotein, whose overexpression at protein level do not match neither with the extent of mRNA overexpression, nor with the frequency of genetic amplifications (7,11).

In addition to cell culture and mouse models (3,4,8,12,13), the role of MYC has been widely studied in *Drosophila*, where the conserved homolog of MYC, dMyc regulates tissue growth and animal size (14,15). In particular, overexpression of dMyc induces growth of cells of the imaginal discs, which are the organs giving rise to wings in adult fly (14). Importantly, dMYC can complement mammalian MYC *in vivo* (13) implying high degree of functional conservation. In humans, MYC is a master regulator of malignant growth. However, MYC protein levels exceeding the optimal proliferation promoting levels primes both normal and cancer cells to apoptosis (2,3,5,12). The principle of MYC-mediated apoptosis priming was originally revealed by findings showing that highly overexpressed transgenic MYC initiates both proliferation and apoptosis programs in pancreatic islet cells. However, MYC

overexpression was capable to drive tumourigenesis only in the context of efficient apoptosis suppression (12). More recently, the *in vivo* importance of MYC expression levels in defining the balance between proliferation and apoptosis was validated by allelic series of inducible MYC expression (3). In addition to spontaneous apoptosis, high MYC levels prime tumour cells to apoptosis induction by drugs that interfere with replication and cell division, such as topoisomerase inhibitors or taxanes (2,16,17). Indeed, MYC is an important determinant of *in vivo* cell survival both during development, and in response to cancer therapy (4). However, how MYC protein levels are controlled endogenously to maintain an optimal MYC balance is incompletely understood.

UBR5 (Ubiquitin protein ligase E3 component n-recognin 5) is an evolutionary conserved E3 ubiquitin ligase that destabilize proteins with N-terminal recognition sequences exposed by proteolytic cleavage (18,19). Recently UBR5 has been shown to target substrates also through other recognition mechanisms than N-terminal recognition (20). UBR5 is essential for mammalian development (21), and has been linked to both pro-tumourigenic and tumor-suppressor activities (19,21-23). However, the mechanism by which UBR5 would promote tumor growth are unclear. It is also unclear how UBR5 may have pro-tumorigenic role in human cancer cells (19,22-24), whereas it has tumor suppressor activity in *Drosophila* (25,26).

Here, we have identified UBR5 as an FBXW7-independent ubiquitin ligase and rheostat for MYC. Consistent with tumor suppressive activity of UBR5 in

Drosophila, loss of UBR5 induced overgrowth of *Drosophila* wing imaginal disc epithelium in a dMyc-dependent manner. On the contrary, UBR5-mediated MYC suppression was found to protect the cancer cells from apoptosis priming. Further, our data reveal genetic co-amplification of *UBR5* and *MYC* in several solid human cancers; and demonstrate functional relevance of reciprocal protein level regulation between these two cancer genes in defining the apoptosis sensitivity of p53-mutant breast cancer cells.

Materials and methods

Cell culture and transfection

HCC38, HCC1937 and HCC1395 cell lines were obtained from American Type Culture Collection (ATCC). Osteosarcoma-MYC-off cell line(27) was a generous gift from Professor Dean Felsher (Stanford University). HeLa, U2OS, T98G, HEK293, Osteosarcoma-MYC-off, MDA-MB-468 and MDA-MB-231 cell lines were cultured in DMEM (Sigma). HCC38, HCC1937 and IMR-32 cell lines were cultured in RPMI (ATCC-modified vision, Thermo Fisher Scientific). MCF10A cells were cultured as described previously (8). The cell lines were authenticated by ATCC, European Collection of Authenticated Cell Cultures (ECACC) or at Institut für Rechtsmedizin, Universität Würzburg. All the cell lines were tested negative for Mycoplasma during the period of this study. Drosophila S2 cells were cultured in Schneider's Drosophila Medium (Thermo). All growth mediums were supplemented with 10% heat-inactivated FBS (Gibco), 2 mmol/L L-glutamine, and penicillin (50 units/mL)/streptomycin (50 mg/mL).

GFP-UBR5, GFP-UBR5-ΔHECT, Flag-UBR5, and Flag-UBR5-ΔHECT were kind gifts from Darren Saunders & Charles Watts(28,29). V5-MYC, V5-MYC^{T58A} and have been described previously (10). Flag-MYC plasmids and HA-MYC (1-262) were from Prof. Bruno Amati. HA-MYC-WT and HA-MYC mutants were kind gifts from Prof. William P. Tansey. HA-ubiqiuitin was a kind gift from Prof. Lea Sistonen. Plasmids were transfected with Lipofectamine® 2000 Transfection Reagent (Thermo Fisher Scientific) according to the manufacturer’s instructions. After 48 hours transfection, cell lysate was collected. Small interfering RNA (siRNA) transfections were performed with

Oligofectamine™ Transfection Reagent (Thermo Fisher Scientific) following to the manufacturer's protocol. Three days after transfections, cells were harvested for analysis. siRNA target sequences are in supplementary table 1. For double-stranded RNA (dsRNA) mediated RNAi in Drosophila S2 cells, the DNA fragment of hyd was amplified with primers flanked by T7 promoter, and dsRNA was produced using the TranscriptAid T7 High yield Transcription Kit (Thermo). To knock down Hyd, S2 cells were cultured with 5 ug/ml dsRNA for 120h.

Immunoblotting and immunoprecipitation

The following are antibodies used for western blot: UBR5 (sc-515494, Santa cruz), MYC (ab32072, Abcam), cleaved PARP (ab32064, Abcam), BIM (2933, Cell signaling), Vinculin (sc-25336, Santa cruz), GAPDH (5G4-6C5, HyTest Ltd), HA (3724, Cell signaling), Flag (F3165, Sigma), GFP (sc-9996, Santa cruz), GST (sc-138, Santa cruz), V5 (R960-25, Invitrogen), Histone H3 (ab1791, Abcam) and Lys48-Specific antibody (05-1307, Millipore). Secondary antibodies are from Dako (P0447 and P0399). Densitometric analysis of the blots was performed using ImageJ. For immunoprecipitation, the cells were lysed in IP buffer (150mM NaCl, 1% NP-40, 50mM Tris pH 8.0) supplemented with protease and phosphatase inhibitors. Cell lysates were centrifuged and immunoprecipitated with the indicated antibodies for 2 h at 4 °C, following by adding Protein A-Sepharose or protein G-Sepharose beads (Sigma) overnight. The beads were washed with IP buffer, boiled in SDS sample buffer and analysed by immunoblotting. MYC (N-262, sc-764), and V5 agarose (A7345, Sigma) were used for immunoprecipitation.

To immunoprecipitate dMyc, lysates were incubated 2 hours with anti-dMyc beads. Anti-dMyc beads were made from rabbit anti-dMyc antibody (Santa Cruz) and 50% protein A Sepharose beads (Amersham). Immunoprecipitates were washed five times with NP-40 lysis buffer, boiled in 2X SDS sample buffer, and resolved on 8% SDS-PAGE for analysing via Western blotting. Immunoprecipitated Myc was detected using mouse anti-Myc antibody (a kind gift from Dr. Peter Gallant).

Ubiquitination assays

For ubiquitination assay in denaturating condition, HEK293 cells transfected with relevant plasmids were lysed in a buffer containing 6 M guanidinium-HCl, 0.1 M Na_2HPO_4, 0.1 M NaH_2PO_4, 0.01 M Tris-HCl (pH 8), 5 mM imidazole and 10 mM β-mercaptoethanol (β-ME). The lysates were incubated with Ni-NTA agarose beads (Qiagen) at 4 °C overnight. The beads were washed once with a buffer containing 6 M guanidinium-HCl, 0.1 M Na_2HPO_4, 0.1 M NaH_2PO_4, 0.01 M Tris-HCl (pH 8) and 10 mM β-ME, and twice with a buffer containing 8 M urea, 0.1 M Na_2HPO_4, 0.1 M NaH_2PO_4, 0.01 M Tris-HCl (pH 8), 10 mM β-ME and 0.1% Triton X-100. His-Ub-conjugated proteins were eluted using a buffer containing 200 mM imidazole, 0.15 M Tris (pH 6.7), 30% glycerol, 0.72 M β-ME and 5% SDS. *In vitro* ubiquitination assays were performed in reactions containing 2 µg ubiquitin (Boston Biochem), 2 mM ATP, 80 ng hUBE1 (Boston Biochem), 2 µg UbcH5c (Boston Biochem), recombinant GST-MYC and GFP-UBR5 purified from HEK293 cells, in a buffer with 800 mM Tris-HCl (pH 7.5), 200 mM $MgCl_2$ and 12 mM DTT. The reactions were incubated at 37 °C for 90 minutes, followed by separation in Mini-

PROTEAN TGX precast gels (Biorad). The samples were analyzed by Western blotting using GFP and GST antibodies.

Immunofluorescence staining

Cells plated on chambered coverslip (80826, Ibidi) were transfected with scrambled siRNA or UBR5 siRNA. After 72 hours transfection, the cells were fixed with 4% paraformaldehyde 15 minutes under room temperature, and then cells were permeabilized with 0.5% Triton X-100 in PBS on ice for 5 minutes. Next, the cells were blocked by 10% normal goat serum (ab7481, Abcam) diluted in PBS for 30 minutes, and followed by incubating the primary antibodies anti-UBR5 (sc-515494, Santa cruz) and anti-MYC(ab32072, Abcam) overnight at 4°C. Subsequently, cells were washed with PBS and incubated with secondary antibodies, Alex Fluor 594 goat anti-Mouse IgG (A-11005, Invitrogen) and Alex Fluor 488 goat anti-rabbit IgG (A-11008, Invitrogen) for 1 hour under room temperature. After secondary antibody incubation, the cells were washed with PBS and nuclei were stained with DAPI (D1306, Invitrogen) in PBS at RT for 10 min. Images were acquired with confocal microscope (LSM780, Carl Zeiss).

***Drosophila* genetics**

Fly stocks used in this study are: Myc RNAi (VDRC 2947), hyd mutant allele K3.5(30) and MARCM82b (a kind gift from Dr. Osamu Shimmi). To induce MARCM clones in developing wing discs(31), larvae were heat-shocked for one hour at 37°C at 72 hours after egg laying. Wing imaginal discs were dissected from late third instar larvae, fixed in 4% formaldehyde for 30 min,

after washing in PBT (0.3% Triton X 100 in PBS), samples were mounted with Vectashield Mounting Medium with DAPI (Mediq), and imaged using a Zeiss LSM 700 microscope. Clone roundness was analyzed as described earlier (32). Volume per cell and pH3 positive cells were counted using Imaris software. To induce MARCM clones in larvae fat body, larvae were heat-shocked for one hour at 37°C at 24 hours after egg laying. Fat bodies were dissected from third instar larvae, fixed in 4% formaldehyde for 30 min, and washed in PBT (0.3% Triton X 100 in PBS). After blocking in 5% BSA in PBT for 3 hours at RT, primary antibody (anti-FBL, 1:500, Abcam) was incubated at 4 C o/n. Primary antibody were washed with PBT and secondary antibody (anti-mouse Alexa fluor 647, Life Technologies) was incubated for 4 hours at RT. After three washes, samples were mounted with Vectashield Mounting Medium with DAPI (Mediq), and imaged using a Zeiss LSM 700 microscope.

Full genotypes in Fig 3d:

yw, hsFLP/+; Tub-G4, UAS-mCD8 GFP/+; FRT82b, Tub-Gal80/FRT82, hydK3.5

Full genotypes in Fig 3e and f:

Ctrl: yw, hsFLP/+; Tub-G4, UAS-mCD8 GFP/+; FRT82b, Tub-Gal80/FRT82b

Myc RNAi: yw, hsFLP/+; Tub-G4, UAS-mCD8 GFP/Myc RNAi; FRT82b, Tub-Gal80/FRT82b

hyd mutant: yw, hsFLP/+; Tub-G4, UAS-mCD8 GFP/+; FRT82b, Tub-Gal80/FRT82, hyd K3.5

hyd mutant, Myc RNAi: yw, hsFLP/+; Tub-G4, UAS-mCD8 GFP/Myc RNAi; FRT82b, Tub-Gal80/ FRT82b, hyd K3.5

Breast cancer IHC and IF analysis

Tissue material was treated according to standard histology practice, i.e. fixed in buffered formalin (pH 7.0) and embedded into paraffin blocks. Tissue microarrays (TMAs) were prepared by collecting two 1.5 mm diameter tissue cores from the representative tumor area, defined by an experienced breast cancer pathologist (PK), of each breast cancer patient. Both immunohistochemistry (IHC) and double immunofluorescence (IF) were performed on sections cut at 3.5 µm. For MYC (ab32072, Abcam, Y69), IHC was performed with Lab Vision Autostainer 480 (Thermo-Fisher Scientific, Fremont, CA, USA) and detected with PowerVision+ polymer kit (DPVB+110HRP; Immunovision Technologies, Vision Biosystems, Norwell, MA, USA) according to standard protocol with diaminobenzidine as chromogen. Before staining, tissue sections were deparaffinized and treated twice for 7 min each in Target Retrieval Solution, pH 9 (S2367, Dako, Glostrup, Denmark) in a microwave oven for antigen retrieval. MYC antibody was applied at a dilution of 1:250. An automated immunostaining machine Discovery XT (Roche Diagnostics/Ventana Medical Systems, Tucson, AZ, USA) was used for UBR5 (sc-515494, Santa Cruz Biotechnology) IHC and UBR5/MYC double IF. Deparaffinization, epitope retrieval (standard option, Cell Conditioning 1 reagent, 950-124, Roche/Ventana) and primary antibody incubation (40 min at 37° C, dilution 1:500 for UBR5-IHC, and 1:1000 and 1:50 for UBR5 and MYC, respectively, for double-IF) were done on the platform. OmniMap HRP (760-4310, Roche/Ventana) and ChromoMap DAB Kit (760-159, Roche/Ventana) were applied for detection of UBR5 IHC. For double IF, OmniMap HRP (Roche/Ventana, 760-4310 and 760-4311 for anti-

279 mouse and anti-rabbit, respectively) together with Rhodamine and FAM
280 fluorescent substrates (Roche/Ventana, 760-233 and 760-243, respectively)
281 were used. Finally, IF slides were mounted applying ProLong® Gold antifade
282 reagent with DAPI (P36935, Molecular Probes by LifeTechnologies). Two
283 slides were stained as controls for double IF. One, by replacing UBR5 primary
284 antibody, and the other, by replacing MYC primary antibody with antibody
285 diluent.
286

Results

UBR5 suppress MYC protein expression

We conducted a screen for ubiquitin ligases that regulate MYC protein levels using a library of siRNAs targeting 591 ubiquitin ligases (Fig. 1A). To focus on ubiquitin ligases that would not regulate MYC stability via the important MYC ubiquitin ligase FBXW7 (9,10,34), the siRNA library was screened against U2OS cells stably expressing MYCT58A mutant (threonine 58 mutated to alanine) that is resistant to FBXW7-mediated destabilization (9,10). 48 hours after siRNA transfection, cells were treated for 3.5 hours with cycloheximide to emphasize the impact of protein stability, and immunofluorescence (IF) detection of MYC was thereafter used as a read-out in a high-content imaging-based assay (Fig. 1A). Among a small group of siRNAs consistently affecting MYCT58A levels (Table S2), the HECT-domain containing E3 ligase UBR5 (alias EDD) was the only E3 ligase affecting only protein levels but not mRNA levels (Fig. S1A), and was therefore selected for further validation experiments.

Physical association between endogenous UBR5 and MYC in HeLa cell nuclei was confirmed by proximity ligation analysis (PLA) (Fig. 1B). The specificity of the PLA reaction was confirmed by staining with PLA secondary antibodies alone (Fig. S1B), and by a clear decrease of positive MYC-UBR5 PLA signals (Fig. 1B), and of UBR5 immunofluorescence signal (Fig. S1C, D) by siRNA treatments. Whereas MYC and UBR5 siRNA treatments exclusively

decreased the number of nuclear PLA signals, they did not affect cytoplasmic signals (Fig. 1B).

To confirm FBXW7-independent function of UBR5, we studied whether MYC binding to UBR5 is affected by MYC T58A mutation, that abolishes recognition by FBXW7 (7,9,35). As a result, GFP-UBR5 associated equally efficiently with both forms of MYC (Fig. 1C). Lack of interaction between overexpressed GFP and MYC was controlled separately (Fig. S1E). Additionally, UBR5 overexpression reduced the levels of MYC T58A and WT MYC to a similar degree (Fig. 1D). Importantly, mutant UBR5 lacking the ubiquitin ligase HECT domain did not reduce the MYC levels (Fig. 1D).

By using different MYC fragments (36, 37), we delineated aminoacids 181-189 of MYC as the minimal candidate region for MYC-UBR5 association (Fig. 1E and S1F). Importantly, the MYC mutant deficient in UBR5 binding (d127-189) repeatedly showed higher protein expression than either WT MYC, or the N-terminal MYC mutants (Fig. 1E and Fig. S1G), and was resistant to inhibition by UBR5 overexpression (Fig. S1G).

The effects of UBR5 depletion on endogenous MYC protein levels in HeLa cells was confirmed by immunoblot analysis using six independent UBR5 siRNA sequences (Fig. 1F). However, MYC did not regulate UBR5 mRNA or protein expression (Fig. S1H, I). In addition to HeLa cells, endogenous MYC protein induction by UBR5 inhibition was confirmed in T98G glioblastoma, and MDA-MB-231 breast cancer cells, and in immortalized MCF-10A mammary

epithelial cells (Fig. 1G). In addition, we performed RNA-sequencing analysis of HeLa cells depleted of MYC or UBR5 (Fig. S1I). By gene set enrichment analysis (GSEA), we found that UBR5 depletion induces expression of same MYC target signature that is suppressed by MYC depletion (Fig. 1H). A heatmap of the individual genes regulated to opposite direction with UBR5 or MYC siRNA is shown in figure 1I, and the genes are listed in supplementary table 3.

UBR5 is a MYC ubiquitin ligase

UBR5 depletion induced a robust increase in the levels of MYC protein but its impact on the MYC mRNA levels was minimal (Fig. 2A). Furthermore, UBR5 depletion significantly increased MYC protein expression when ectopic MYC mRNA expression was induced by gradual removal of doxycycline from mouse OS-Tet-Off-MYC cells (27), further supporting a regulation at post-translational levels (Fig. 2B). Consistent with UBR5 regulating MYC protein stability, UBR5 depletion stabilized MYC in a cycloheximide chase experiment in HeLa (Fig. 2C and S2A), and in U2OS cells (Fig. S2B, C). Regarding other MYC family members, endogenous MYCN was also stabilized by UBR5 siRNA in IMR-32 neuroblastoma cells (Fig. S2D, E). Further validating the UBR5 degron on MYC, MYC d129-189 mutant was insensitive to UBR5-mediated destabilization (Fig. S2F, G). Notably, depletion of either FBXW7 or UBR5 increased endogenous MYC stability, and co-depletion of both ubiquitin ligases further increased MYC stability (Fig. 2D and S2H, I). Additive effects of UBR5 and FBXW7 inhibition on MYC stability were confirmed by Eilers

laboratory by using independent UBR5 and FBXW7 siRNAs (Fig. S2J). These results clearly support independent roles for UBR5 and FBXW7 in MYC protein regulation.

Consistent with ubiquitination-mediated regulation of MYC by UBR5, MYC inhibition by overexpression of the wild-type UBR5 was rescued by co-treatment with proteasome inhibitor MG132 (Fig. 2E, F). Moreover, in ubiquitination assays, only overexpression of the wild-type UBR5, but not the HECT mutant, induced ubiquitination of V5-MYC (Fig. 2G). Reciprocally, siRNA-mediated depletion of UBR5 potently inhibited MYC ubiquitination (Fig. 2H). Moreover, we found that UBR5-induced ubiquitination of MYC is at least in part via K48-linked ubiquitin chains (Fig. 2I), which are mainly responsible for proteasomal degradation of proteins. Additionally, increased covalent attachment of ubiquitin to MYC in UBR5 overexpressing cells was confirmed by performing the His-ubiquitin pull-down under denaturating conditions (Fig. S2K). Finally, by using purified UBR5 and MYC proteins, we demonstrate that UBR5 can *in vitro* conjugate ubiquitin to the 1-262 fragment of recombinant MYC, spanning the UBR5 degron (Fig. 2J).

Together, these data identify UBR5 as a novel MYC ubiquitin ligase that regulates MYC stability independently of FBWX7.

UBR5 controls *in vivo* tissue growth in dMyc-dependent manner in *Drosophila*

To explore the possible functional conservation, and the role of the UBR5-MYC axis in normal tissue homeostasis *in vivo*, we utilized a *Drosophila melanogaster* model. The *Drosophila* UBR5 ortholog Hyd (Hyperplastic discs) was originally identified as a putative tumor suppressor (19,22,26,38). RNAi-mediated depletion of Hyd in *Drosophila* S2 cells (Fig. S3A) led to elevated levels of *Drosophila* MYC (dMyc) protein (Fig. 3A), whereas the mRNA levels of dMyc did not correlate with dMyc protein induction (Fig. 3B). Importantly, the levels of Hyd RNA reduction by RNAi was directly reflected in a comparable 2-fold induction of dMyc protein levels (Fig. S3A and 3A). Similar to regulation of MYC target genes by UBR5 in human cells (Fig. 1H,I), Hyd depletion induced mRNA expression of two dMyc targets eIF6 and Nop5 (Fig. 3C and S3B), and protein expression of Fibrillarin (Fig. 3D,E), which is a well-established MYC target in both human and *Drosophila*.

The *Drosophila* models allows the use of somatic recombination to generate clones of mutant tissue in an otherwise heterozygous background. Clones of $hyd^{K3.5}$ mutant cells generated during mid larval development (72 h after egg laying) showed a phenotype clearly visible in the adult wings (Fig. S3C). Wings with *hyd* mutant clones were irregular, lacking the normal flat wing morphology, and displaying uneven wing margins and veins (Fig. 3F and S3C, see arrows). Notably, this irregular wing phenotype was strongly suppressed by simultaneous knockdown of dMyc in the mutant clones (Fig. 3F and S3C).

The use of the MARCM system to generate mutant clones allowed us to GFP label, and to visualize the tissue morphology of the wing imaginal discs, the larval wing precursors (31). Control and Myc RNAi clones appeared

morphologically normal with GFP positive clones having a normal but irregular shape (Fig. 3G, H). In contrast, *hyd* mutant clones had a round morphology with clusters of cells growing out from the epithelial plane (Fig. 3G, H), which was confirmed by quantification of the clone roundness (Fig. 3H). The roundness phenotype in wing clones has been earlier validated to mark activated Ras-MAPK-MYC signalling (32). Most importantly, simultaneous RNAi-mediated knockdown of dMyc suppressed the round morphology, thus rescuing the phenotype of the *hyd* mutant clones, which was further confirmed by quantification (Fig. 3H).

To dissect the relevance of cell size and proliferation (15) in dMyc-dependent regulation of *Drosophila* tissue growth by Hyd, we first analyzed cell size in *hyd* mutant clones. *hyd* mutant cells were significantly larger than controls and this phenotype was fully suppressed by simultaneous knockdown of dMyc (Fig. 3I). We also observed higher percentage of phospho-histone H3, a marker commonly used as a proxy for cell proliferation, in the *hyd* mutant clones, but this phenotype was independent of dMyc expression (Fig. S3D). Thus, we conclude that the increased cell size, and roundness (established mark of activated MYC signaling (32)), but not proliferation, are dependent on dMyc in *hyd* mutant *Drosophila* tissues.

These results demonstrate that in *Drosophila* suppression of dMyc protein expression is a critical part of growth control by the ortholog of UBR5 *in vivo*.

UBR5 suppresses MYC-mediated apoptosis priming in cancer cells

Proliferation and apoptosis are known to be governed by different levels of MYC (2-5,12,17,39,40). In HeLa cells, UBR5 depletion decreased colony growth (Fig. 4A), suggesting that MYC levels may have reached the levels that prime them to apoptosis. This was confirmed by the increased PARP cleavage, and by the induction of Caspase-3/7 activity in at least a fraction of UBR5-depleted cells (Fig. 4B, C). To evaluate the balance between MYC-regulated proliferation and apoptosis, we titrated UBR5 siRNA and studied the dose-dependent correlation between MYC levels, and induction of cleaved-PARP or inhibition of a directly MYC-regulated cell cycle inhibitor p21 (41). Interestingly, while p21 suppression was almost maximal already with 10 nM of UBR siRNA (Fig. 4D, E), cleaved-PARP continued to increase with higher UBR5 siRNA concentrations (Fig. 4D, E). These results indicate that both proliferation and apoptosis priming are initiated upon increased MYC expression, and that loss of cells in colony growth assay (Fig. 4A) is a result of MYC expression exceeding the apoptosis-inducing levels. Importantly, apoptosis priming by UBR5 inhibition was highly dependent on MYC induction. First, both PARP cleavage, and caspase-3/7 activation were fully rescued by concurrent MYC depletion (Fig. 4F, G). Second, UBR5 depletion was unable to induce PARP cleavage in OS-Tet-Off-MYC cells with maximal doxycycline-elicited MYC suppression (Fig. 4H).

Mechanistically MYC overexpression can induce apoptosis either via ARF-MDM2-p53 dependent pathway (2,42,43), or by engaging pro-apoptotic BH3 protein BIM in a p53-independent manner (40,41,44). Supportive of a BIM-

dependent mechanism, we found that co-depletion of BIM abolished apoptosis induction in UBR5-depleted cells (Fig. 4I). Moreover, BIM induction by UBR5 siRNA was abolished by co-depletion of MYC (Fig. 4J). On the other hand, cells depleted of p53 displayed equally potent colony growth reduction, and PARP cleavage by UBR5 depletion than control cells (Fig S4A, B). Further, endogenous inactivating p53 mutations did not prevent MYC-dependent PARP cleavage, or BIM induction, in UBR5 siRNA transfected breast cancer cells (Fig. S4C).

MYC-dependent apoptosis priming is particularly relevant for increased sensitivity of cancer cells to antimitotic agents such as taxanes (17), and to drugs that interfere with high replication activity, such as topoisomerase I inhibitors (camptothecins) (16). Accordingly, growth inhibition in UBR5 depleted cells was greatly potentiated by treatment of cells with either taxol or camptothecin, at doses that alone do not induce massive loss of cells (Fig 4K, S4D). Importantly, MYC expression was essential for hypersensitivity of UBR5 depleted cells to both taxol and camptothecin (Fig. 4K, L) since drug responses were indistinguishable between the control cells, and cells treated with UBR5+MYC siRNA in a concentration-dependent manner (Fig. S4E).

Collectively these results demonstrate that UBR5 suppresses MYC-mediated but p53-independent apoptosis priming in cancer cells.

Co-amplification of *UBR5* and *MYC* protects breast cancer cells from MYC-mediated priming to drug-induced apoptosis

The results above suggest that expression of UBR5 might provide a selective advantage for cancer cells by suppressing MYC-mediated apoptosis priming. The cancer types in which this biology is particularly relevant would be expected to exhibit co-expression of *Ubr5* and *Myc* at mRNA level, but $UBR5^{high}/MYC^{low}$ status at protein level (see cartoon Fig. 5A). Across 672 cell lines and over 20 different cancer types (45), a weak but statistically significant correlation between *Ubr5* and *M*yc mRNA expression levels was detected (Pearson correlation 0.21, $p<0.01$; Fig. S5A). Significant positive correlation between *Myc* and *Ubr5* mRNA expression was observed in four cancer types, ovary, lymphoid, breast and pancreas (Fig. S5A). Importantly, MYC has been closely linked to progression of all these four cancer types, and existing data indicate a growth-promoting role of UBR5 in at least pancreatic, ovary, and breast cancer (22,23,46,47).

We noted that both *UBR5* and *MYC* genes are located in the long arm of chromosome 8, suggesting a model where *UBR5* co-amplification with *MYC* might provide means to control excessive MYC protein levels, and thereby protect cells from apoptosis priming (Fig. 5A). Examination of TCGA cancer patient amplification data for *UBR5* and *MYC* in the four cancer types with an evidence for mRNA co-expression (Fig. S5A), revealed that the percentage of patient samples with single amplification of either *UBR5* or *MYC* ranged from 2 % in lymphoid cancers, to 44 % in ovary cancers (Table 1). Interestingly, co-amplification of *UBR5* and *MYC* appeared in 65% of breast, 42% of ovary, and 39% of pancreas cancers. On the other hand amplification of *UBR5* alone

was a very rare event in any of these cancer types. Breast cancers were the only cancer type in which the percentage of cancers with co-amplification exceeded the percentage of cancers with *MYC* amplification alone (Table 1), indicating that *UBR5* co-amplification, and UBR5 protein expression, may provide a particular benefit for breast cancer cells with *MYC* amplification.

To assess functional relevance of UBR5 in co-amplified breast cancer cells, we correlated breast cancer cell line UBR5 essentiality index (zGARP score)(48), with *MYC/UBR5* gene copy numbers in these same cells. Notably, we observed a statistically significant correlation between the zGARP score and *MYC/UBR5* gene copy numbers in cell lines with zGARP score < -1.5 (Fig. 5B). Next, we tested the xenograft growth potential of UBR5-depleted HCC38 cells. Transient siRNA transfection of HCC38 cells resulted in at least 10 days suppression of UBR5 protein expression validating the approach for xenograft experiment (Fig. S5B). Remarkably, UBR5 depletion from HCC38 even with transient siRNA transfection was sufficient to almost entirely inhibit tumor growth in mice (Fig. 5C). *In culture*, we observed that UBR5 depletion in both HCC38 and HCC1937 cells did induce MYC protein levels and MYC-dependent apoptosis priming (as observed by PARP cleavage) (Fig. 5D, and S5C). As HCC38 harbors p53 R273L mutation in the DNA-binding domain, these results further strengthen the p53-independence of apoptosis priming induced by loss of UBR5.

Patients with co-amplification of *MYC* and *UBR5* had significantly poorer overall survival than patients without neither of the genes amplified (Fig. S5D). However, as survival of patients with *MYC* amplification alone did not

statistically differ from survival of patients with co-amplification, we conclude that potential relevance of UBR5 mediated MYC suppression in co-amplified breast cancers could rather associate with the resistance to therapy-induced apoptosis. Fully supporting the hypothesis, UBR5 depletion from HCC38 cells with *MYC/UBR5* co-amplification resulted in modest MYC-dependent inhibition of colony growth, but led to a very potent MYC-dependent sensitisation of cell killing to both FDA approved topoisomerase I inhibitors, Irinotecan and Topotecan (Fig. 5E; the full concentration-dependent dose-response curves are show in Figure S5E,F). We also confirmed a significant MYC-dependent priming to Taxol-induced cell killing by UBR5 inhibition in HCC38 cells (Fig. 5F).

Together these results identify co-amplification of *MYC* and *UBR5* in large fraction of MYC-dependent solid cancer types. Results further indicate that *UBR5* co-amplification with *MYC* might be relevant to suppress drug-induced apoptosis in p53-mutant breast cancer cells.

UBR5 dominates MYC protein levels in individual breast cancer cells *in vivo*

Finally, we searched for *in vivo* evidence that UBR5 suppresses MYC protein expression in human breast cancer tissue. Consistently with published results (49), *MYC* amplification was most frequent in basal-type breast cancers, and this was also the subtype where co-amplification was most pronounced (Fig. S6A). Based on this information, we used tissue microarray of 345 samples

from 197 human basal-type breast cancers to examine correlation between UBR5 and MYC protein expression *in vivo.* The IHC staining was optimized such that intensities from 0 to +++ were reliably observed with both UBR5 and MYC antibodies (Fig. S6B). Consistently with the hypothesis of UBR5 dominating MYC expression, the percentage of staining positive cells (+, ++, or +++) was greater for UBR5 than for MYC in 78% of the samples (Fig. S6C). This finding was re-confirmed by using an independent set of human breast cancer samples (n = 74), and a different staining protocol in Klefström laboratory (Fig. S6D).

When tumor samples were examined by using adjacent 3 μM tissue sections, we observed an apparent dichotomy of UBR5 and MYC protein levels in individual basal type breast cancer cells (Fig. S6E; regions 1 and 2). Importantly, while UBR5 and MYC positivity is almost exclusively confined to tumor cells (Fig. S6E, F), we could identify some immune-like cells that also show very clear inverse correlation between UBR5 and MYC expression (Fig. S6E). These results further emphasize the general importance of our results across different cell types.

To quantitatively validate these observations, we developed a double immunofluorescence (IF) staining protocol. Antibody specificity was demonstrated by siRNA-mediated depletion (Fig. 1B and S1D), and by secondary antibody only control staining (Fig. S6G). Further, the double-IF was optimized so that maximal staining intensities were practically indistinguishable with both UBR5 and MYC antibodies (Fig. S6H). Thus,

individual cells could be categorized into $MYC^{high}/UBR5^{low}$ (green), $UBR5^{high}/MYC^{low}$ (red) and $MYC^{high}/UBR5^{high}$ (yellow) phenotypes (Fig. 6A). Staining of TMA cores revealed that basal-type breast cancers could be broadly divided into either UBR5 dominant or MYC dominant, or to cancers that showed both UBR5 or MYC dominant cells (Fig. 6B). Supporting the IHC results, UBR5 was overall more highly expressed than MYC across all quantified 18 667 cells (Fig. 6C). Pairwise comparison of UBR5 and MYC intensities in all quantified individual cells demonstrated that in 64% of cells UBR5 was more highly expressed than MYC, whereas 27% of cells were MYC dominant (Fig. 6D). Fully consistent with a dichotomy of UBR5 and MYC expression (Fig. S6E), only 9% of the cells displayed equal UBR5 and MYC protein expression intensities (yellow) (Fig. 6D).

To demonstrate statistical significance of UBR5 dominance over MYC at single cell level, we performed a pairwise density distribution analysis of UBR5 dominance from all 18 667 individual cells. To this end, MYC intensity in each individual cell was subtracted from UBR5 intensity from the same cell, and distribution of the resulting pairwise intensity difference was blotted on a scale that corresponded to actual IF intensity levels (Fig. 6E, S6H). The null hypothesis was that UBR5 and MYC expression would have been equal, and thus pairwise UBR5-MYC intensity difference would have centered around zero. The results however show that cells with either UBR5 dominance (UBR5 intensity-MYC intensity > 0), or MYC dominance (UBR5 intensity-MYC intensity < 0), constitute two different populations (Fig. 6E). Moreover, the median of UBR5 intensity-MYC intensity was strongly positive, and the

density of UBR5 dominant cells is significantly higher than with MYC dominant cells. Thereby these results confirm that UBR5 dominates MYC protein expression in a majority of individual basal type breast cancer cells *in vivo*. This conclusion was further supported by regression analysis between UBR5 and MYC IF intensities in individual cells that was clearly indicative of negative correlation between these proteins at the single cell level (Fig. 6F). Interestingly, all cells having lower than approximately 30% of maximal UBR5 intensity had strong MYC expression (Fig. 6F), indicating that other mechanisms are not capable of effectively suppressing MYC in basal type breast cancers in the absence of UBR5. Based on our other results (Fig. 4K,l, 5E,F, and S5E,F), these $UBR5^{low}/MYC^{high}$ cells would constitute the Irinotecan and Topotecan sensitive cell population *in vivo.*

This first single cell analysis of protein expression of MYC and its ubiquitin ligase demonstrate that UBR5 and MYC are exclusive for high level protein expression in most of the basal type breast cancer cells *in vivo.* As high UBR5 expression dominated high MYC expression in most of the cells, these results provide *in vivo* relevance for the role of UBR5 in negative regulation of MYC.

Discussion

UBR5 regulates various cellular processes (19,28,50,51), but the role for UBR5 in both inhibiting and promoting organismal growth has been enigmatic (19,22,23,25,46,50,52). The observed overgrowth in *Drosophila* epithelial tissue in *hyd* mutant flies via dMyc is fully consistent with the reported growth suppressor role of Hyd (19,25). On the other hand, UBR5-mediated suppression of MYC-induced apoptosis observed in cancer cell lines is well in accordance with previously reported oncogenic activities of UBR5 (22,23). In support of *in vivo* relevance of these observations, we demonstrate both that UBR5 suppresses dMyc activity in wing development (Fig. 3), and that in most of the basal type breast tumor cells UBR5 dominates MYC protein levels at the single cell level (Fig. 6C-F, S6E). Directly supportive of oncogenic role of UBR5 in human cancer cells *in vivo*, UBR5 depleted basal-like breast cancer cells with *UBR5/MYC* amplification failed to grow as xenograft tumors (Fig. 5C). Collectively, we conclude that UBR5 finetunes MYC protein expression to the levels that balance cell growth and survival (Fig. 6G).

Although the conclusions that lower levels of MYC would be more beneficial for the tumor are somewhat counter intuitive, they are fully in accordance with previous results using transgenic MYC mouse models. These studies have demonstrated the importance of MYC protein levels in controlling the delicate balance between proliferation and apoptosis (2,3,12). Whereas these previous studies convincingly demonstrated that the dose of MYC protein is critical to sustain maximal fitness of the cell, identification of endogenous candidate rheostat proteins such as UBR5, that define MYC levels *in vivo*,

may help in future to better understand how the balance between MYC-mediated regulation of cell growth and apoptosis is defined by cell intrinsic mechanisms. Notably, in addition to demonstrating both the *in vitro* and the *in vivo* relevance of UBR5-MYC axis, we also show that opposite to some of the other UBR5 functions that are strictly restricted to certain cell types (21,52), we failed to identify a cell type in which UBR5 inhibition would have not increased MYC protein expression. Therefore, we anticipate these findings to have wide-reaching implications in different biological systems.

Co-amplification with *MYC* introduces UBR5 as so far unique MYC ubiquitin ligase. Based on amplification frequencies of *UBR5* and *MYC*, it is clear that *UBR5* amplification alone does not provide significant benefit for breast cancer cells. However, also *MYC* amplification without *UBR5* amplification was only seen in 28% of the samples with any amplifications, whereas co-amplification was observed in 70% of all cases in which *MYC* was amplified (Table 1). Together with results that *MYC/UBR5* co-amplification frequency correlates with essentiality of UBR5 for breast cancer cell survival (Fig.5B), and with UBR5-mediated protection of *MYC/UBR5* co-amplified breast cancer cells drug-induced apoptosis (Fig. 5E,F), we postulate that co-amplification of *UBR5* gives a survival benefit to *MYC* amplified cells for example under drug-induced stress conditions. An additional discovery with high cancer relevance was p53-independence of MYC-mediated apoptosis in UBR5 inhibited cells. As cancer cells with combination of *MYC*-amplification and p53-mutation constitutes the most malignant cell population in many cancers, identification of a ubiquitin ligase regulating MYC-mediated apoptosis in this type of cells

constitutes a major advancement with profound future potential. Intriguingly, opposite to breast cancers, *UBR5* amplifications were not observed in lymphoid cancers. The discrepancy between solid and lymphoid cancers in regards to their UBR5 status is illustrated also by the fact that frequent *UBR5* mutations (which are predicted to disrupt E3 ligase activity) are observed in mantle cell lymphoma (24). Thereby, it is possible that whereas UBR5 promotes oncogenesis in solid cancers by decreasing MYC-mediated apoptosis, in hematological cancers UBR5 functions as a tumor suppressor, and this activity is lost by frequent loss-of-function mutations.

Even though the study did not directly address potential role of UBR5 as a cancer therapy target, our results proposes for a possible strategy to unleash MYC´s pro-apoptotic activity for cancer therapy. Based on our data, we envision that UBR5 inhibition could harmonize the tumor cells to more uniformly express MYC protein at the levels that would predispose the cells to cell killing by cancer drugs. Optimally this could prevent re-appearance of those cancer cell populations that were protected from the initial drug-induced apoptosis due to their low MYC expression. In addition to the presented data, this model is supported by recent demonstration of MYC as a major *in vivo* determinant of taxane response (17), and the data that pretreatment mitochondrial priming correlates with clinical response to cytotoxic chemotherapy in cancer (53). Unfortunately, testing of this hypothesis is currently unfeasible because no small molecule inhibitors for UBR5 are available. Another potential clinical application of the data is use of breast

cancer tissue UBR5^{low}/MYC^{high} IHC status for patient stratification to Topoisomerase I inhibitor therapies.

In summary, this study characterizes UBR5 as a novel MYC ubiquitin ligase controlling MYC activity in development of epithelial tissue *in vivo,* and in p53-mutant cancer cells. Collectively the results provide a novel molecular explanation for both the tumor suppressive, as well as tumor promoting roles of UBR5. Co-amplification of *UBR5* with *MYC* indicates for a concept that at certain circumstances it is beneficial for cancer cells to gain strong oncogenic activity, but simultaneously assure that this activity is kept in leash by co-amplification of the natural suppressor mechanism.

Acknowledgements:

The authors thank Prof. Johanna Ivaska and Prof. Lea Sistonen for valuable comments to the manuscript. The authors thank for Prof. Dean Felsher providing osteosarcoma-MYC-off cell line. Prof. Saunders, Watts Amati, Sears and Tansey are thanked for plasmids and Peter Gallant for the anti-dMyc antibody. Birgit Samans is thanked for the support with the statistical analysis of the high-content siRNA screen image assay and Karolina Pavic for purification of recombinant MYC protein. We thank greatly Taina Kalevo-Mattila for excellent technical help, Sinikka Collanus for help in IF and IHC, Samu Kurki, Eliisa Löyttyniemi, Srikar Nagelli and Teemu Daniel Laajala for statistical analysis of IHC data. Personnel of Cell Imaging Core facility, Finnish Functional Genomics Centre, and Medical Bioinformatics Centre of Turku Bioscience Centre (supported by Biocenter Finland and Elixir-Finland) are all thanked for their valuable contributions. This study was supported by funding from Sigrid Juselius Foundation, Finnish Cancer Associations, Deutsche Forschungsgemeinschaft grant (Ei222/12-1), Academy of Finland (286767 and 312439), Foundation Martin Escudero, Finnish Cultural Foundation South-Western Regional Fund, Instrumentarium Science Foundation, Maud Kuistila Memorial Foundation, and Ella and Georg Enhrooth Foundation, K.Albin Johanssons Foundation, Paolo Foundation, and South-Western Finland Cancer Society.

References

1. Mertins P, Mani DR, Ruggles KV, Gillette MA, Clauser KR, Wang P*, et al.* Proteogenomics connects somatic mutations to signalling in breast cancer. Nature **2016**;534:55-62

2. McMahon SB. MYC and the control of apoptosis. Cold Spring Harb Perspect Med **2014**;4:a014407

3. Murphy DJ, Junttila MR, Pouyet L, Karnezis A, Shchors K, Bui DA*, et al.* Distinct thresholds govern Myc's biological output in vivo. Cancer Cell **2008**;14:447-57

4. Sarosiek KA, Fraser C, Muthalagu N, Bhola PD, Chang W, McBrayer SK*, et al.* Developmental Regulation of Mitochondrial Apoptosis by c-Myc Governs Age- and Tissue-Specific Sensitivity to Cancer Therapeutics. Cancer Cell **2017**;31:142-56

5. Nieminen AI, Eskelinen VM, Haikala HM, Tervonen TA, Yan Y, Partanen JI*, et al.* Myc-induced AMPK-phospho p53 pathway activates Bak to sensitize mitochondrial apoptosis. Proc Natl Acad Sci U S A **2013**;110:E1839-48

6. Thomas LR, Tansey WP. Proteolytic control of the oncoprotein transcription factor Myc. Adv Cancer Res **2011**;110:77-106

7. Farrell AS, Sears RC. MYC degradation. Cold Spring Harb Perspect Med **2014**;4

8. Myant K, Qiao X, Halonen T, Come C, Laine A, Janghorban M*, et al.* Serine 62-Phosphorylated MYC Associates with Nuclear Lamins and Its

762 Regulation by CIP2A Is Essential for Regenerative Proliferation. Cell reports
763 **2015**;12:1019-31
764 9. Welcker M, Orian A, Jin J, Grim JE, Harper JW, Eisenman RN*, et al.*
765 The Fbw7 tumor suppressor regulates glycogen synthase kinase 3
766 phosphorylation-dependent c-Myc protein degradation. Proc Natl Acad Sci U
767 S A **2004**;101:9085-90
768 10. Yeh E, Cunningham M, Arnold H, Chasse D, Monteith T, Ivaldi G*, et al.*
769 A signalling pathway controlling c-Myc degradation that impacts oncogenic
770 transformation of human cells. Nat Cell Biol **2004**;6:308-18
771 11. Levens D. You Don't Muck with MYC. Genes Cancer **2010**;1:547-54
772 12. Pelengaris S, Khan M, Evan GI. Suppression of Myc-induced apoptosis
773 in beta cells exposes multiple oncogenic properties of Myc and triggers
774 carcinogenic progression. Cell **2002**;109:321-34
775 13. Trumpp A, Refaeli Y, Oskarsson T, Gasser S, Murphy M, Martin GR*, et*
776 *al.* c-Myc regulates mammalian body size by controlling cell number but not
777 cell size. Nature **2001**;414:768-73
778 14. Grifoni D, Bellosta P. Drosophila Myc: A master regulator of cellular
779 performance. Biochimica et biophysica acta **2015**;1849:570-81
780 15. Johnston LA, Prober DA, Edgar BA, Eisenman RN, Gallant P.
781 Drosophila myc regulates cellular growth during development. Cell
782 **1999**;98:779-90
783 16. Rohban S, Campaner S. Myc induced replicative stress response: How
784 to cope with it and exploit it. Biochimica et biophysica acta **2015**;1849:517-24
785 17. Topham C, Tighe A, Ly P, Bennett A, Sloss O, Nelson L*, et al.* MYC Is
786 a Major Determinant of Mitotic Cell Fate. Cancer Cell **2015**;28:129-40

787 18. Varshavsky A. The N-end rule pathway and regulation by proteolysis.
788 Protein Sci **2011**;20:1298-345
789 19. Shearer RF, Iconomou M, Watts CK, Saunders DN. Functional Roles
790 of the E3 Ubiquitin Ligase UBR5 in Cancer. Mol Cancer Res **2015**;13:1523-32
791 20. Shen Q, Qiu Z, Wu W, Zheng J, Jia Z. Characterization of interaction
792 and ubiquitination of phosphoenolpyruvate carboxykinase by E3 ligase UBR5.
793 Biol Open **2018**;7
794 21. Saunders DN, Hird SL, Withington SL, Dunwoodie SL, Henderson MJ,
795 Biben C*, et al.* Edd, the murine hyperplastic disc gene, is essential for yolk
796 sac vascularization and chorioallantoic fusion. Mol Cell Biol **2004**;24:7225-34
797 22. Clancy JL, Henderson MJ, Russell AJ, Anderson DW, Bova RJ,
798 Campbell IG*, et al.* EDD, the human orthologue of the hyperplastic discs
799 tumour suppressor gene, is amplified and overexpressed in cancer.
800 Oncogene **2003**;22:5070-81
801 23. Liao L, Song M, Li X, Tang L, Zhang T, Zhang L*, et al.* E3 Ubiquitin
802 Ligase UBR5 Drives the Growth and Metastasis of Triple-Negative Breast
803 Cancer. Cancer Res **2017**;77:2090-101
804 24. Meissner B, Kridel R, Lim RS, Rogic S, Tse K, Scott DW*, et al.* The E3
805 ubiquitin ligase UBR5 is recurrently mutated in mantle cell lymphoma. Blood
806 **2013**;121:3161-4
807 25. Callaghan MJ, Russell AJ, Woollatt E, Sutherland GR, Sutherland RL,
808 Watts CK. Identification of a human HECT family protein with homology to the
809 Drosophila tumor suppressor gene hyperplastic discs. Oncogene
810 **1998**;17:3479-91

811 26. Mansfield E, Hersperger E, Biggs J, Shearn A. Genetic and molecular
812 analysis of hyperplastic discs, a gene whose product is required for regulation
813 of cell proliferation in Drosophila melanogaster imaginal discs and germ cells.
814 Developmental biology **1994**;165:507-26
815 27. Jain M, Arvanitis C, Chu K, Dewey W, Leonhardt E, Trinh M*, et al.*
816 Sustained loss of a neoplastic phenotype by brief inactivation of MYC.
817 Science **2002**;297:102-4
818 28. Gudjonsson T, Altmeyer M, Savic V, Toledo L, Dinant C, Grofte M*, et*
819 *al.* TRIP12 and UBR5 suppress spreading of chromatin ubiquitylation at
820 damaged chromosomes. Cell **2012**;150:697-709
821 29. Henderson MJ, Russell AJ, Hird S, Munoz M, Clancy JL, Lehrbach
822 GM*, et al.* EDD, the human hyperplastic discs protein, has a role in
823 progesterone receptor coactivation and potential involvement in DNA damage
824 response. The Journal of biological chemistry **2002**;277:26468-78
825 30. Lee JD, Amanai K, Shearn A, Treisman JE. The ubiquitin ligase
826 Hyperplastic discs negatively regulates hedgehog and decapentaplegic
827 expression by independent mechanisms. Development **2002**;129:5697-706
828 31. Lee T, Luo L. Mosaic analysis with a repressible cell marker for studies
829 of gene function in neuronal morphogenesis. Neuron **1999**;22:451-61
830 32. Prober DA, Edgar BA. Interactions between Ras1, dMyc, and dPI3K
831 signaling in the developing Drosophila wing. Genes Dev **2002**;16:2286-99
832 33. Schindelin J, Arganda-Carreras I, Frise E, Kaynig V, Longair M,
833 Pietzsch T*, et al.* Fiji: an open-source platform for biological-image analysis.
834 Nature methods **2012**;9:676-82

835 34. Welcker M, Clurman BE. FBW7 ubiquitin ligase: a tumour suppressor
836 at the crossroads of cell division, growth and differentiation. Nat Rev Cancer
837 **2008**;8:83-93
838 35. Gregory MA, Qi Y, Hann SR. Phosphorylation by glycogen synthase
839 kinase-3 controls c-myc proteolysis and subnuclear localization. The Journal
840 of biological chemistry **2003**;278:51606-12
841 36. Sanchez-Arevalo Lobo VJ, Doni M, Verrecchia A, Sanulli S, Faga G,
842 Piontini A*, et al.* Dual regulation of Myc by Abl. Oncogene **2013**;32:5261-71
843 37. Herbst A, Salghetti SE, Kim SY, Tansey WP. Multiple cell-type-specific
844 elements regulate Myc protein stability. Oncogene **2004**;23:3863-71
845 38. Martin P, Martin A, Shearn A. Studies of l(3)c43hs1 a polyphasic,
846 temperature-sensitive mutant of Drosophila melanogaster with a variety of
847 imaginal disc defects. Developmental biology **1977**;55:213-32
848 39. Freie BW, Eisenman RN. Ratcheting Myc. Cancer Cell **2008**;14:425-6
849 40. Muthalagu N, Junttila MR, Wiese KE, Wolf E, Morton J, Bauer B*, et al.*
850 BIM is the primary mediator of MYC-induced apoptosis in multiple solid
851 tissues. Cell reports **2014**;8:1347-53
852 41. Seoane J, Le HV, Massague J. Myc suppression of the p21(Cip1) Cdk
853 inhibitor influences the outcome of the p53 response to DNA damage. Nature
854 **2002**;419:729-34
855 42. Sherr CJ. Tumor surveillance via the ARF-p53 pathway. Genes &
856 Development **1998**;12:2984-91
857 43. Finch A, Prescott J, Shchors K, Hunt A, Soucek L, Dansen TB*, et al.*
858 Bcl-xL gain of function and p19 ARF loss of function cooperate oncogenically
859 with Myc in vivo by distinct mechanisms. Cancer Cell **2006**;10:113-20

44. Hemann MT, Bric A, Teruya-Feldstein J, Herbst A, Nilsson JA, Cordon-Cardo C*, et al.* Evasion of the p53 tumour surveillance network by tumour-derived MYC mutants. Nature **2005**;436:807-11

45. Klijn C, Durinck S, Stawiski EW, Haverty PM, Jiang Z, Liu H*, et al.* A comprehensive transcriptional portrait of human cancer cell lines. Nature biotechnology **2015**;33:306-12

46. O'Brien PM, Davies MJ, Scurry JP, Smith AN, Barton CA, Henderson MJ*, et al.* The E3 ubiquitin ligase EDD is an adverse prognostic factor for serous epithelial ovarian cancer and modulates cisplatin resistance in vitro. British journal of cancer **2008**;98:1085-93

47. Mann KM, Ward JM, Yew CC, Kovochich A, Dawson DW, Black MA*, et al.* Sleeping Beauty mutagenesis reveals cooperating mutations and pathways in pancreatic adenocarcinoma. Proc Natl Acad Sci U S A **2012**;109:5934-41

48. Marcotte R, Sayad A, Brown KR, Sanchez-Garcia F, Reimand J, Haider M*, et al.* Functional Genomic Landscape of Human Breast Cancer Drivers, Vulnerabilities, and Resistance. Cell **2016**;164:293-309

49. Dillon JL, Mockus SM, Ananda G, Spotlow V, Wells WA, Tsongalis GJ*, et al.* Somatic gene mutation analysis of triple negative breast cancers. Breast **2016**;29:202-7

50. Sanchez A, De Vivo A, Uprety N, Kim J, Stevens SM, Jr., Kee Y. BMI1-UBR5 axis regulates transcriptional repression at damaged chromatin. Proc Natl Acad Sci U S A **2016**;113:11243-8

883 51. Su H, Meng S, Lu Y, Trombly MI, Chen J, Lin C*, et al.* Mammalian
884 hyperplastic discs homolog EDD regulates miRNA-mediated gene silencing.
885 Mol Cell **2011**;43:97-109
886 52. Kinsella E, Dora N, Mellis D, Lettice L, Deveney P, Hill R*, et al.* Use of
887 a Conditional Ubr5 Mutant Allele to Investigate the Role of an N-End Rule
888 Ubiquitin-Protein Ligase in Hedgehog Signalling and Embryonic Limb
889 Development. PLoS ONE **2016**;11:e0157079
890 53. Ni Chonghaile T, Sarosiek KA, Vo TT, Ryan JA, Tammareddi A, Moore
891 Vdel G*, et al.* Pretreatment mitochondrial priming correlates with clinical
892 response to cytotoxic chemotherapy. Science **2011**;334:1129-33
893 54. Hann SR. Role of post-translational modifications in regulating c-Myc
894 proteolysis, transcriptional activity and biological function. Semin Cancer Biol
895 **2006**;16:288-302
896
897

Table 1 Distribution of amplification rates of MYC and UBR5 in TCGA patient samples in the indicated cancer types

	Breast	Pancreas	Ovary	Lymphoid
Total number of sample	1080	183	579	48
No. of samples with either MYC and/or UBR5 amplifications (% of total)	247 (22.8%)	23 (12.5%)	254 (43.8%)	1 (2%)
Cancers with MYC amplifications only (% of amplifications)	28%	61%	54%	1%
Cancer with UBR5 amplifications only (% of amplifications)	7%	0%	4%	0%
Cancers with MYC/UBR5 co-amplifications (% of amplifications)	65%	39%	42%	0%

Figure legends:

Fig.1 UBR5 negatively regulates MYC protein levels. A, High-content imaging-based screen was performed to identify E3 ubiquitin ligases that regulate MYCT58A. An example of immunofluorescence staining of MYC and a secondary antibody control only is shown. **B**, Proximity ligation assay analysis of the UBR5 and MYC association in HeLa cells transfected with scrambled (Scr), MYC siRNA or UBR5 siRNA. Shown is a quantification of the average number of UBR5-MYC PLA signals per cell in cytoplasm and nucleus. **C**, UBR5, wild-type MYC or MYCT58A mutants were overexpressed in HEK293 cells by transient transfection. Cell lysates were immunoprecipitated with GFP or V5 agarose and interaction was detected with relevant antibodies. The numbers show fold change of relevant proteins. Shown is a representative experiment; n=3. **D**, HEK293 cells were co-

transfected with empty vector, GFP-tagged UBR5, UBR5 mutant, V5-tagged MYC and MYCT58A mutant plasmids. Shown is a representative experiment; n=2. **E**, UBR5, wild-type MYC or MYC mutants were overexpressed in HEK293 cells by transient transfection. Cell lysates were immunoprecipitated with HA antibody and interaction was detected with GFP antibody. Shown is a representative experiment; n=3. **F**, Hela cells were transfected with scrambled (Scr) or 6 different UBR5 siRNAs. After 72 hours, cell lysates were collected to detect MYC expression by western blot. **G**, Effect of UBR5 siRNA on MYC in T98G, MDA-MB-231 and MCF10A cells. **H**, Gene set enrichment analysis (GSEA) of RNA-seq data generated in Hela cells transfected with Scr, UBR5 or MYC siRNAs. NES, normalized enrichment score. **I**, Heatmap illustrating the expression level changes (>2 folds by siUBR5) of genes co-regulated by UBR5 and MYC in (H).

Fig.2 Validation of UBR5 as a MYC ubiquitin ligase. A, MYC mRNA and protein expression in Hela cells transfected with scrambled (Scr) or UBR5 (5#) siRNA. Error bars represent SD (for mRNA expression, n=3; for protein expression, n=14), ***, P < 0.001, ****, P < 0.0001 by student's t-test. **B**, Analysis of MYC expression in mouse osteosarcoma-MYC-off cells transfected with scrambled (Scr) or UBR5 siRNA. **C**, Hela cells transfected with scrambled (Scr) or UBR5 (5#) siRNA for 72 hours were treated with cycloheximide (CHX, 60μg/ml) for indicated time points. For Western blot see Fig S2A. Error bars mean ± SD. *, P < 0.05 by student's t-test (n=3). **D**, Hela cells transfected with indicated siRNAs for 72 hours were treated with cycloheximide (CHX, 60μg/ml) for different time points. For Western blot see

Fig S2I. Error bars mean ± SD. *, P < 0.05 by student's t-test (n=3). **E**, HEK293 cells were co-transfected with GFP-tagged wild type UBR5, UBR5-HECT domain mutant, and V5-tagged MYC plasmid. After 48 hours transfection, the cells were treated with MG132 (20μM) 6 hours. SE and LE represent short and long exposure time. **F**, Quantification of MYC expression from (E). Error bars show SD from 4 independent experiments. *, P < 0.05 by student's t-test. **G**,**H**,**I** HEK293 (G) or HeLa (H,I) cells were co-transfected with indicated plasmids. After 48 hours transfection, the cells were treated with MG132 (20μM) for 6 hours. Immunoprecipitation was performed with anti-V5 agarose. Ubiquitination of MYC was detected by HA antibody (G,H) or ubiquitin K48 specific antibody. **J**, Recombinant GST-MYC (1-262) and GFP-UBR5 purified from HEK293 cells were incubated in *in vitro*-ubiquitination reactions. Samples were analyzed by western blotting using GFP and GST antibodies. **G-J,** Shown is a representative experiment; n=2-3.

Fig. 3 Loss of UBR5 ortholog Hyd drives wing imaginal disc overgrowth in Myc-dependent manner. A, Immunoblot showing immunoprecipitated dMyc levels in S2 cells transfected with Scr or Hyd dsRNA. Kinesin was used as a control for the input. Shown is a representative blot of two experiments with similar results. **B**, Quantitative RT-PCR analysis of dMyc mRNA expression in control and Hyd depleted S2 cells. RP49 was used as a reference gene. Error bar shows SD. n=3. **C**, eIF6 mRNA expression in control and Hyd depleted S2 cells. Error bar shows SD. n=3. *, P < 0.05 by student's t-test. **D**, Loss of Hyd in GFP-labelled fat body mutant clones leads to increase of Fibrillarin expression. **E**, Quantification of (D). The Fibrillarin

level of an adjacent GFP negative cell was used as control. n=10, **, P < 0.01 by student's t-test. **F**, Induction of *hyd* mutant clones leads to uneven wing morphology, which in suppressed by simultaneous knockdown of Myc within the clones. Arrows in magnified image show uneven wing margins and veins. **G**, Loss of Hyd in GFP-labelled mutant clones leads to MYC-dependent overgrowth indicated by roundness, and loss of normal epithelial morphology. Scale bar means 10 μm. **H**, Representative images show clone morphology in wing imaginal discs in control and *hyd* mutant clones. Scale bar means 10 μm. Quantification of the clone roundness was shown. Error bar shows SD. n=30. **, P <0.01 by student's t-test. **I**, Loss of Hyd in GFP-labelled wing disc mutant clones leads to increased cell volume. Simultaneous knockdown of dMyc suppresses this phenotype. n=3, *, P < 0.05 by student's t-test.

Fig. 4 UBR5 suppresses MYC-mediated apoptosis in cancer cells. A, Hela cells transfected with three UBR5 siRNAs were cultured 7 days for colony growth assay. Error bars show SD. n=3. **, P <0.01 by student's t-test. **B**, Hela cells were transfected with two UBR5 siRNAs for 72 hours. Total cell lysates were subjected to immunoblotting with indicated antibodies. **C**, Caspase 3/7 activity was examined in UBR5 depleted Hela cells. Error bars show SD for 7 technical repeats with similar results. **, P <0.01 by student's t-test. **D**, Hela cells were transfected with different concentrations of UBR5 siRNA for 72 hours. Cell lysates were analyzed by western blot with indicated antibodies. **E**, Quantification of MYC, cleared-PARP and p21 expression from (D). Error bars show SD from 2 independent experiments. **F**, Hela cells were transfected with two UBR5 siRNAs, or with combination of UBR5 siRNA and

MYC siRNA for 72 hours. Cell lysates were collected for western blot with indicated antibodies. **G,** Caspase 3/7 activity was examined in Hela cells transfected with indicated siRNAs. Error bars show SD of 2 independent experiments. *, P < 0.05 by student's t-test. **H**, The osteosarcoma-MYC-off cells treated with 20ng/ml doxycycline were transfected with scrambled (Scr) or UBR5 siRNA and cultured in medium with 20ng/ml doxycycline. After 48 hours, medium was changed with or without 20ng/ml doxycycline for culture another 48 hours. **I**, Caspase 3/7 activity was examined in Hela cells transfected with indicated siRNAs. Shown is mean ± SD of 2 independent experiments. *, P < 0.05 by the student's t- test. **J**, Hela cells were transfected with Scr, UBR5 siRNAs, combination of UBR5 and MYC siRNA, and combination of UBR5 and BIM siRNAs. **K**, Colony growth assay were performed in Hela cells transfected with Scr, siUBR5 or combination of UBR5 and MYC siRNAs followed by 24 hours treatment of Taxol (2nM) or CPT (20nM). After 7 days, cells were fixed and stained. **L**, Quantification of drug response fold changes relative to Scr siRNA in (K). Error bars show SEM of 4 independent experiments. *, P < 0.05 by student's t-test.

Fig. 5 *UBR5* and *MYC* are co-amplified in human breast cancer. A, Schematic figure of *UBR5* and *MYC* gene locus in the long arm of chromosome 8 and indicated relationship between their expression at mRNA and protein levels. Whereas mRNA expression is predicted to correlate in co-amplified samples (upward arrows), UBR5 is predicted to suppress MYC protein expression in these samples (opposite direction arrows). **B**, Scatter plot showing the relationship between *UBR5/MYC* co-amplification and *UBR5*

gene essentiality in the breast cancer cell lines. The minimum of *UBR5* and *MYC* amplification levels were correlated against the zGARP scores, a measure of UBR5 essentiality in a shRNA dropout screen. **C**, The volume of tumors isolated from mice on the final day of the experiment (day 28) (n=8). **, P < 0.01 by student's t-test. **D**, *UBR5/MYC* co-amplified HCC1937 or HCC38 cells were transfected with indicated siRNAs. **E**, Colony growth assay of siRNA transfected HCC38 cells was performed following 24 hours treatment with Irinotecan (80nM) or Topotecan (40nM). Error bars show SEM of 2 independent experiments. **F**, Colony growth assay of siRNA transfected HCC38 cells was performed following 24 hours treatment with Taxol (8nm). Error bars show SEM of 3 independent experiments. *, P < 0.05, **, P < 0.01 by student's t-test.

Fig. 6 UBR5 controls MYC protein expression at single cell level in basal type breast cancer *in vivo.* **A**, Intensity of MYC and UBR5 protein from dual immunofluorescence staining was used to categorize individual cells in breast cancer tissues into either MYC or UBR5 dominant. **B**, Dual immunofluorescent staining of UBR5 and MYC in TMA of human basal-type breast cancer. **C**, Quantification of UBR5 and MYC staining at single cell level from 18 667 cells by software FIJI. Error bars mean SD. ****, P < 0.0001. **D,** Pie-chart analysis of distribution of cells based on whether either MYC (green) or UBR5 (red) was expressed at higher level. Cells in which there was < 10% intensity difference between UBR5 and MYC were classified as having equal protein expression (yellow). **E,** Pairwise density distribution analysis of 18 667 individual cells reveals bimodal distribution of UBR5 or MYC dominant cells.

F, Regression analysis between UBR5 and MYC IF intensities in individual cells (n=18 667). **G**, Schematic presentation of UBR5-mediated control of MYC levels critical for proliferation and apoptosis regulation. MYC protein levels accumulate differently between UBR5 high and low expressing cells. In UBR5 low expressing cells (blue area), MYC protein accumulates efficiently due to high protein stability, and high MYC protein expressing cells exceed the apoptosis priming levels. In UBR5 high expressing cells (green area), UBR5 restrains MYC protein accumulation to the levels that maximally support proliferation, but do not exceed the levels that would result in apoptosis priming even with maximal c-Myc mRNA transcription rates.

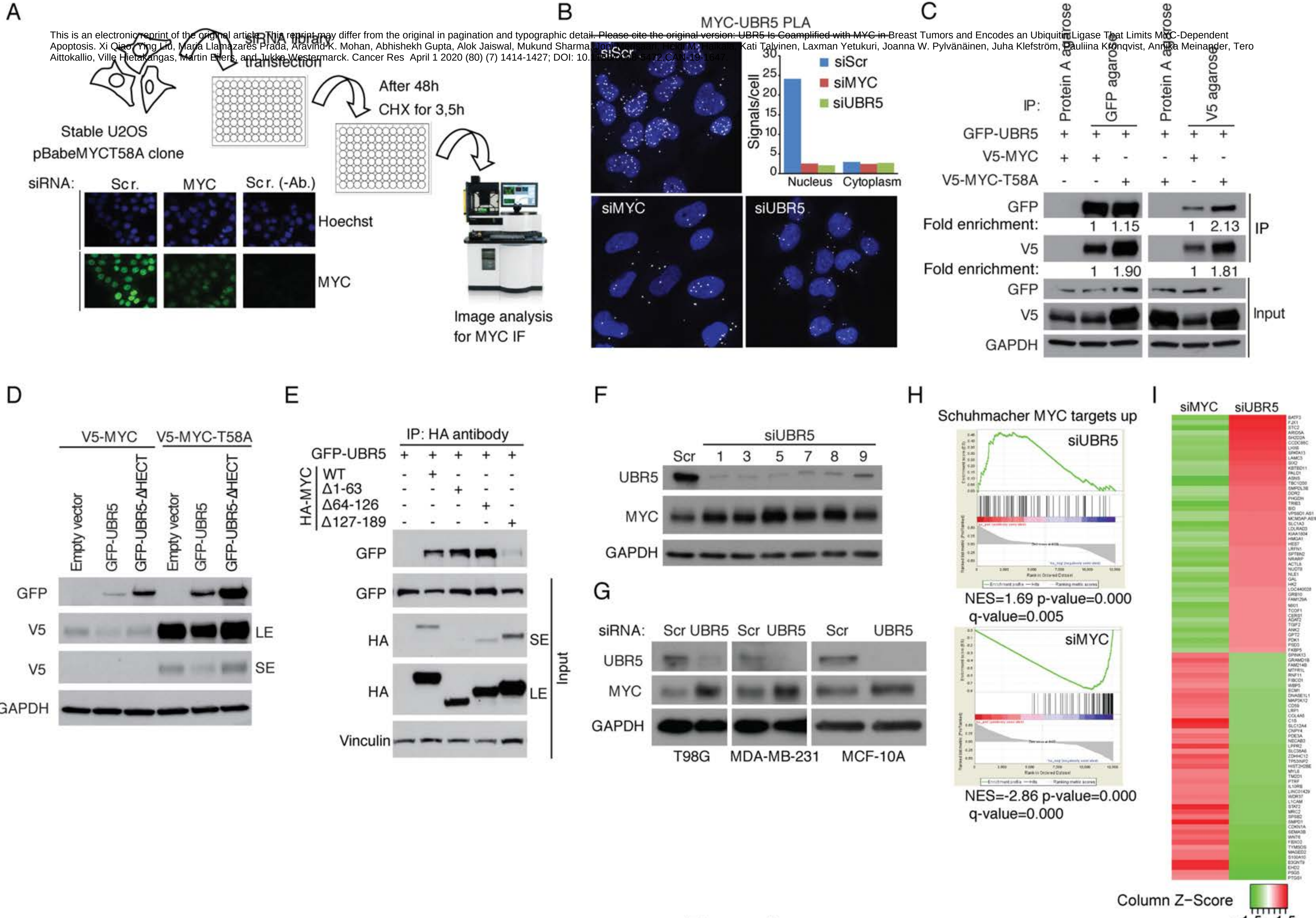

Figure 1

Figure 2

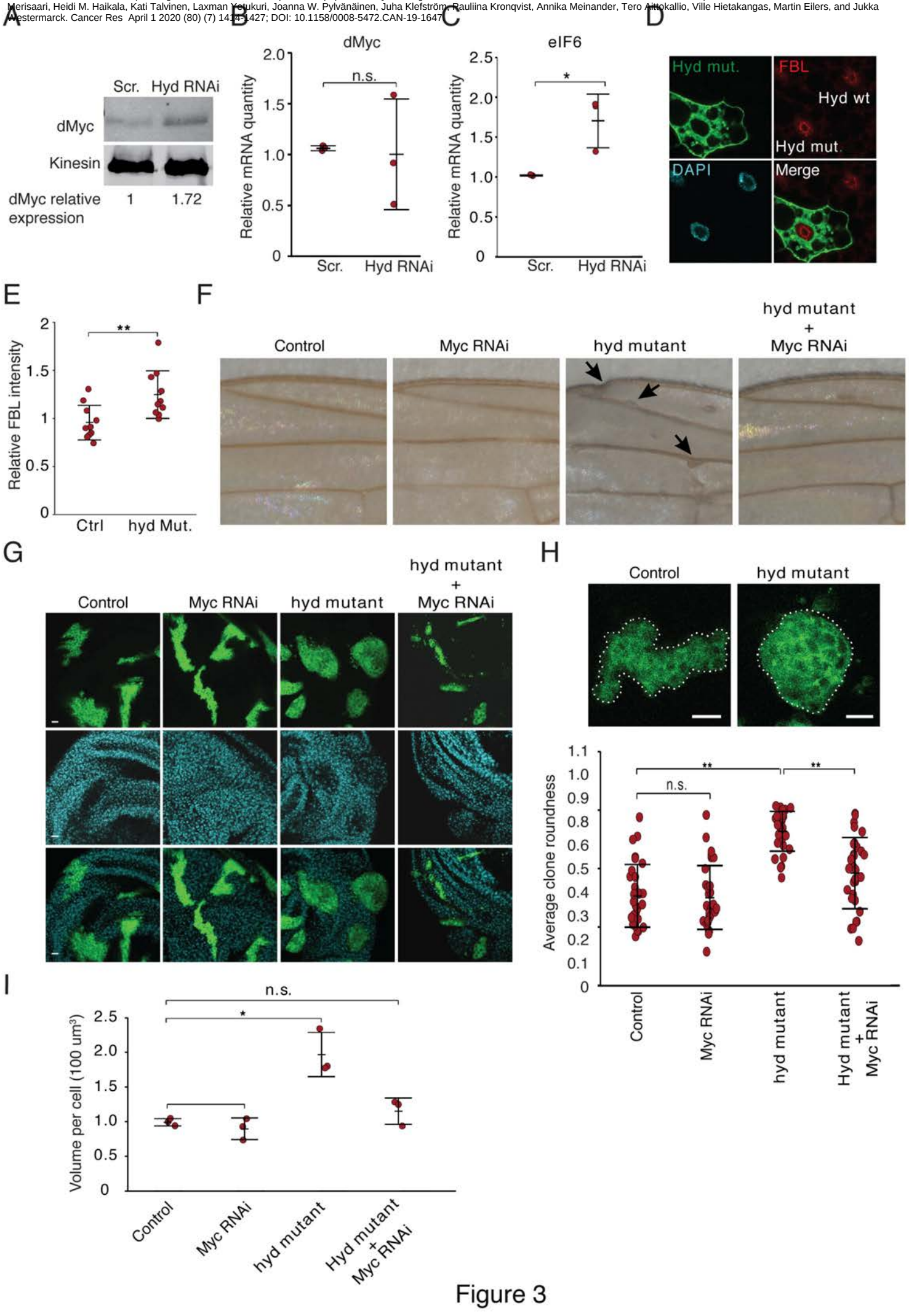

Figure 3

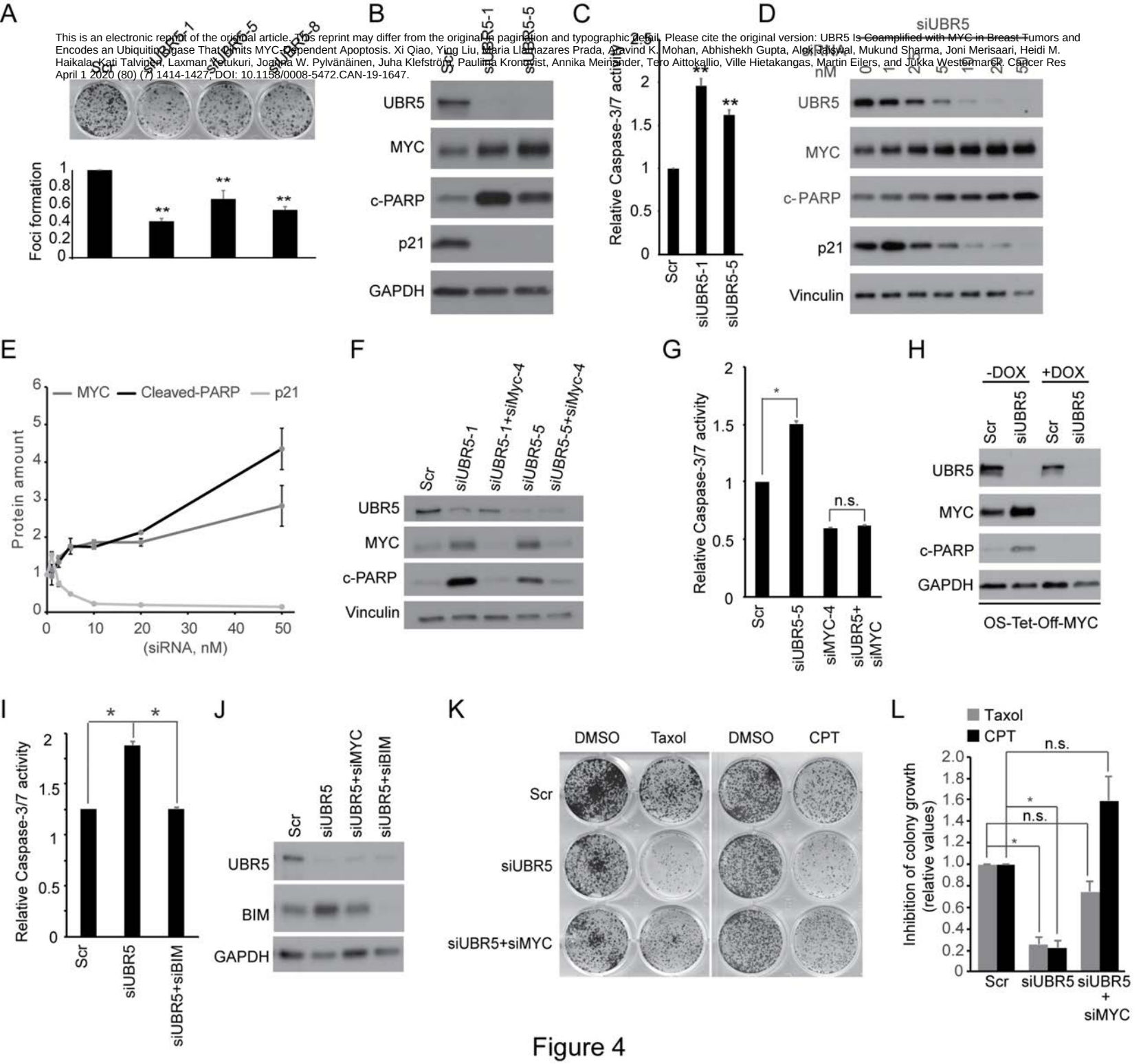

Figure 4

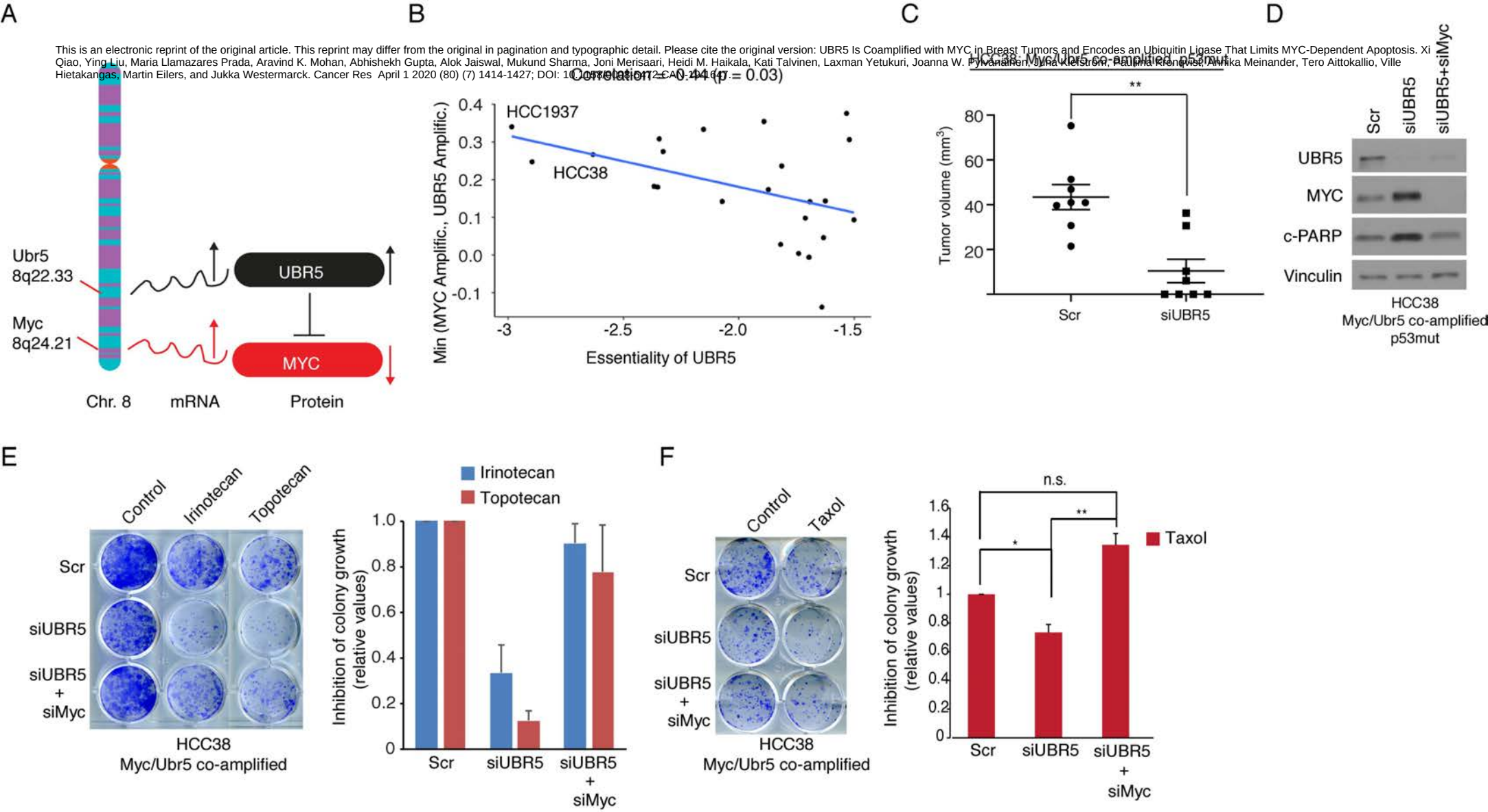

Figure 5

Figure 6

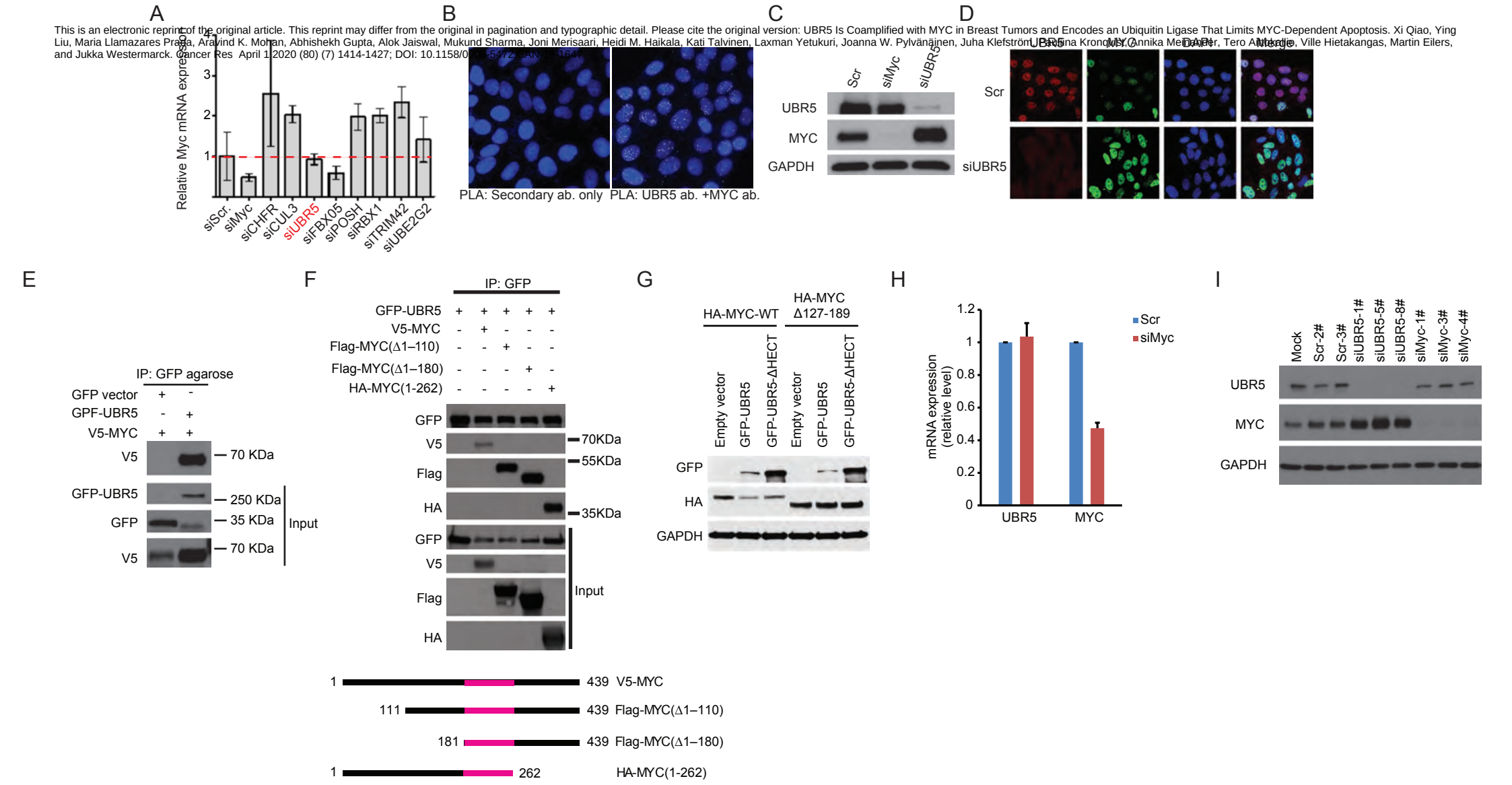

Fig. S1

Fig. S1| A) Validation of candidate E3 ubiquitin ligases identified from high-content imaging-based assay was performed by qRT-PCR. **B)** PLA analysis of the UBR5 and MYC association in HeLa cells. Negative control is without primary antibodies of UBR5 and MYC. **C)** Parallel western blot validation for PLA samples used in Fig. 1b. **D)** Immunofluorescent staining of UBR5 and MYC was done in HeLa cells transfected with scrambled (Scr) or UBR5 (5#) siRNA. **E)** Control experiment to exclude unspecific interaction between eGFP and V5-MYC in a GFP agarose pull-down used in other experiments. **F)** Co-immunoprecipitation was employed to map the interaction area in MYC protein by using MYC deletion constructs transfected in HEK293 cells. The pink shows the minimal common sequence between MYC fragments that was shown to interact with UBR5. **G)** Effect of transiently transfected UBR5 WT or HECT mutant on either wild-type HA-MYC or HA-MYC with 127-189 deletion. **H)** Q-PCR analysis of UBR5 and MYC mRNA expression in either Scr or MYC siRNA transfected HeLa cells after 72 hours. **I)** Western blot validation of UBR5 and MYC inhibition by siRNA (72 h) from HeLa cell cultures parallel to those subjected to RNA-sequencing analysis.

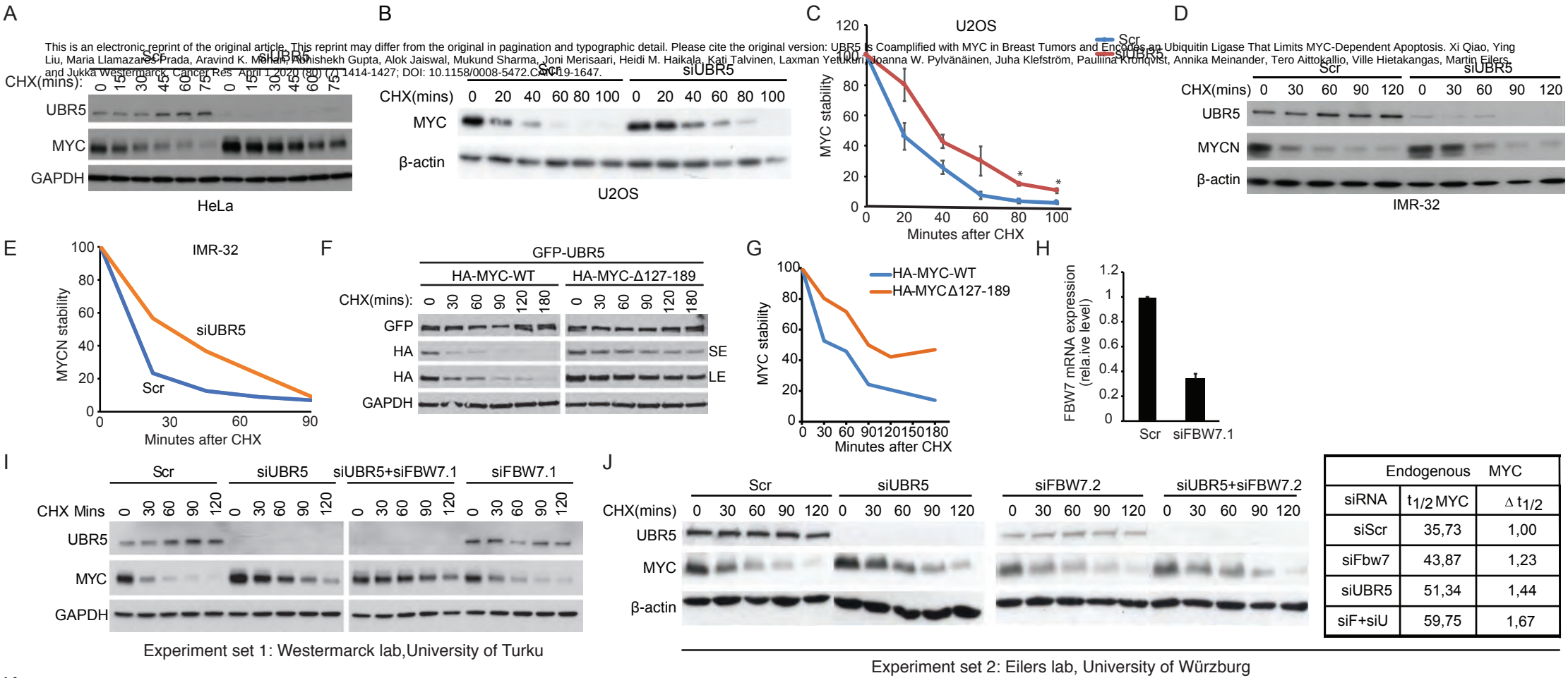

Endogenous MYC		
siRNA	$t_{1/2}$ MYC	$\Delta t_{1/2}$
siScr	35,73	1,00
siFbw7	43,87	1,23
siUBR5	51,34	1,44
siF+siU	59,75	1,67

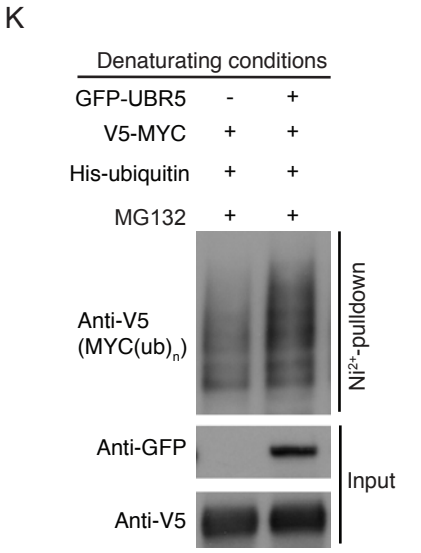

Fig. S2

Fig. S2| **A)** Representative blot of 3 independent experiments for which quantification is shown in Fig. 2c. **B)** U2OS cells transfected with scrambled (Scr) or UBR5 (5#) siRNA were treated with cycloheximide (CHX, 60µg/ml) for indicated time points. Total cell lysates were examined to detect MYC by western blot. **C)** Quantification of MYC expression was done from (B). Error bars show SD from 3 independent experiments. *, P < 0.05 by student's t-test. **D)** IMR-32 neuroblastoma cells transfected with scrambled (Scr) or UBR5 siRNA were treated with cycloheximide (CHX, 60µg/ml) for indicated time points. Total cell lysates were examined to detect MYCN by western blot. **E**) Quantification of MYCN expression was done from (D). **F,G)** HA-MYC-Δ127-189 is resistant to destabilization by UBR5 overexpression **H)** HeLa cells was transfected with FBW7 siRNA for 72 hours to validate the efficiency of siRNA. Error bars mean SD. **I)** Representative blot of 3 independent experiments for which quantification is shown in Fig. 2D. **J)** Repetition of experiment shown in (I) by using independent set of siRNAs and in another research laboratory. **K)** MYC ubiquitination by UBR5 overxpression. Ni^{2+}-pullldown of His-Ubi conjugated proteins was perfomed under denaturating conditions to demonstrate covalent coupling of ubiquitin to MYC, detected by a ladder with anti-V5 antibody.

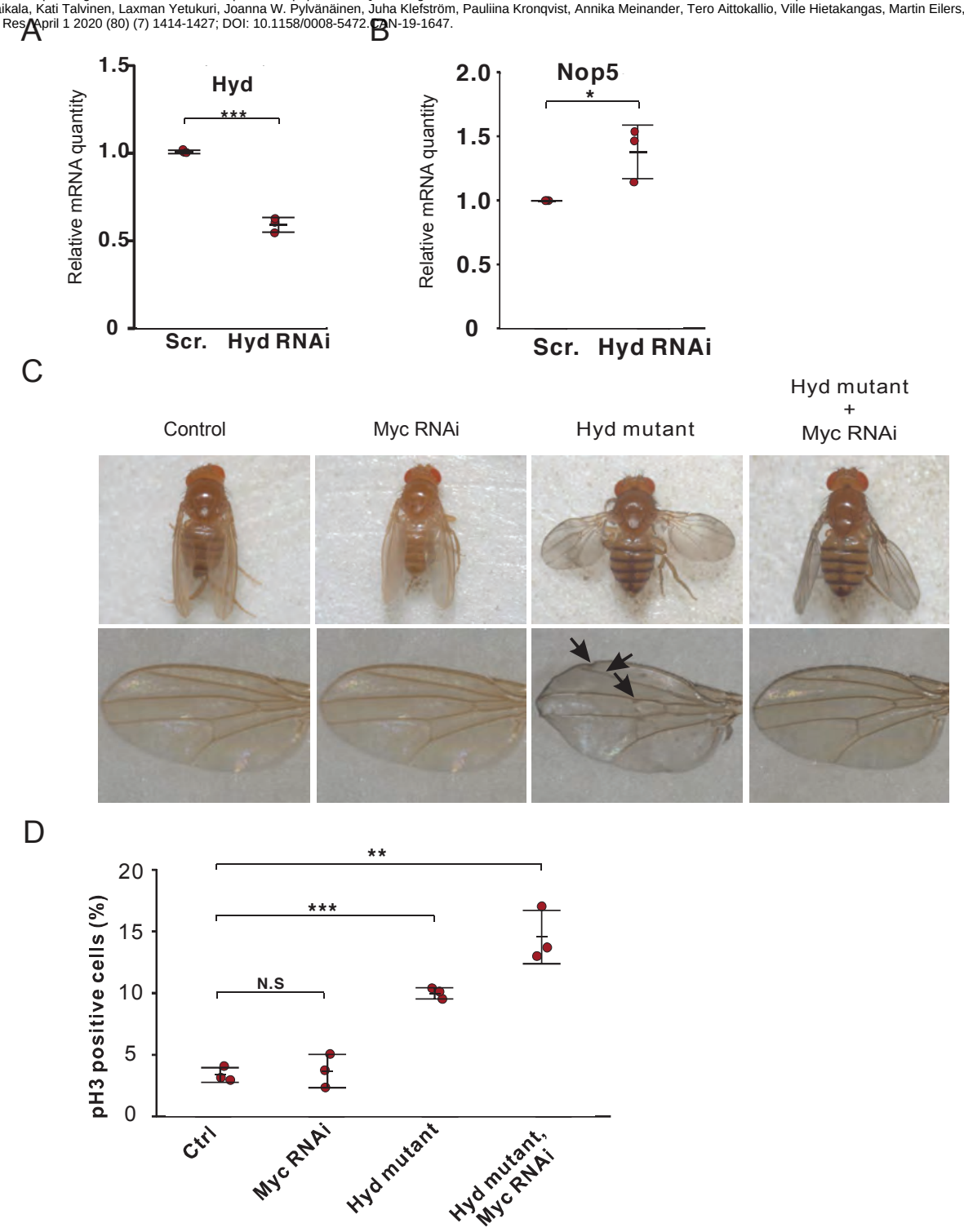

Fig. S3

Fig. S3| A) Quantitative RT-PCR analysis of Hyd expression in control and Hyd depleted S2 cells. RP49 was used as a reference gene. n=3. Error bar means SD. ***, P <0.001 by the student's t-test. **B)** Quantitative RT-PCR analysis of Myc target gene, Nop5 mRNA expression in control and Hyd depleted S2 cells. Error bar means SD. n=3. *, P < 0.05 by student's t-test. **C)** Phenotype changes in the adult wings of indicated drosophila strains. **D)** Loss of Hyd in GFP-labelled wing disc mutant clones leads to Myc-independent increase in phospho-histone H3 levels. Error bar means SD. n=3. ***, P <0.001, **, P <0.01 by student's t-test.

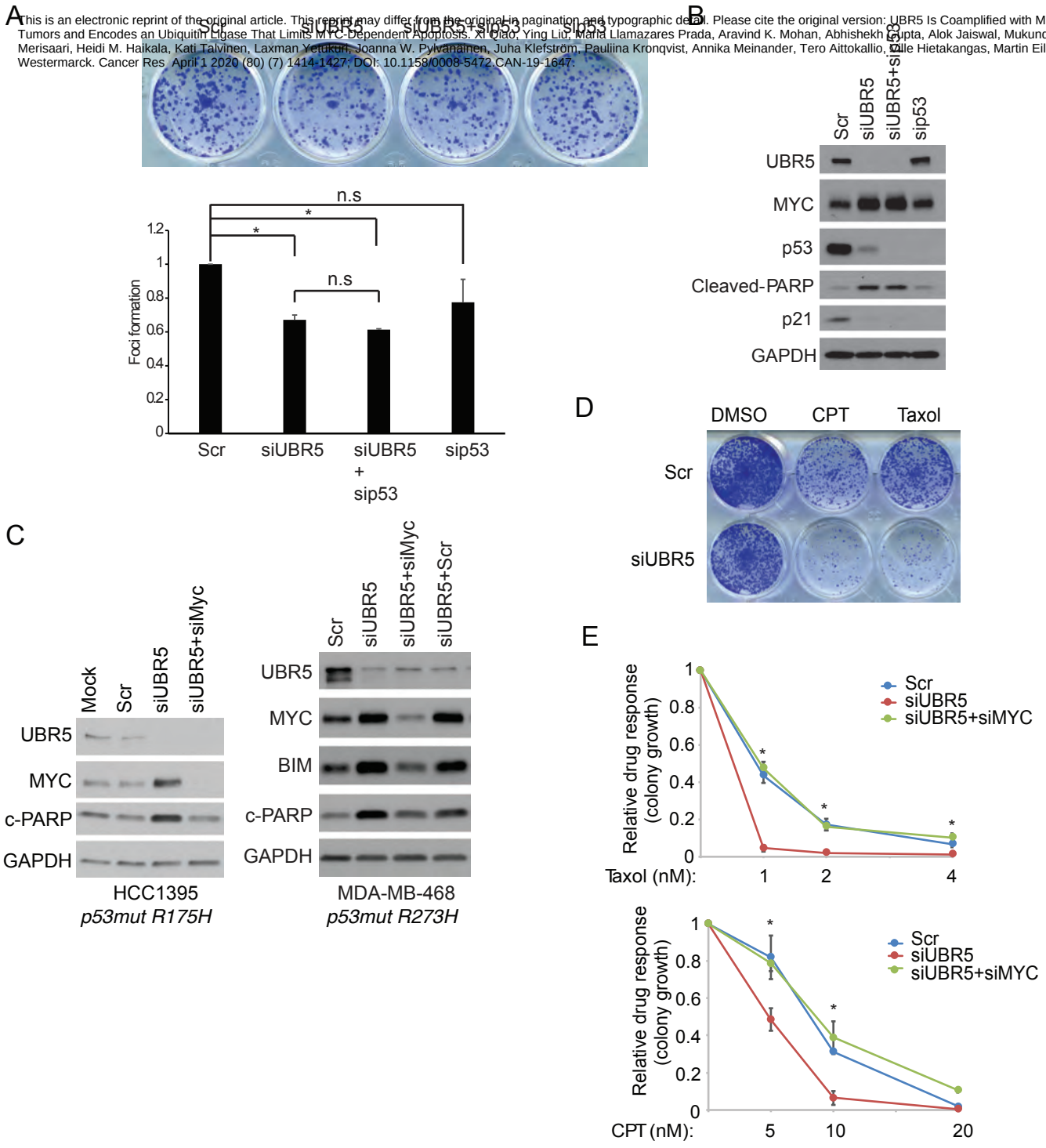

Fig. S4

Fig. S4| A) Colony growth assay was performed in HeLa cells transfected with indicated siRNAs. Error bars show SD (n=3). *, P <0.05 by student's t-test. **B)** Parallel western blot analysis of cell lysates from (A). **C)** UBR5 depletion induces PARP cleavage in two p53 mutant basal-like breast cancer cell lines in MYC-dependent manner. **D)** UBR5 inhibition sensitizes HeLa cells to campthotecin and Taxol. **E-F)** Colony growth assay of siRNA transfected HeLa cells was performed following 24 hours treatment with taxol or camptothecin. Quantification shows relative drug response. Error bars show SD for technical triplicates. *, P <0.05 by student's t-test.

A

Correlation of Ubr5 and Myc mRNA expression in Klijn et al., cell line data

Tumor type		Correlation	p-value
All types	672	0.21	**<0.01**
Brain		0.08	0.67
Skin		0.15	0.37
Ovary		0.36	**0.02**
Lymphoid		0.23	**0.02**
Lung		-0.02	0.81
Kidney		0.38	0.28
Sarcomatiod		0.76	0.05
Stomach		0.32	0.11
Uterus		-0.08	0.9
Colo-rectal		0.04	0.78
Urinary bladder		0.46	0.36
Head-neck		-0.11	0.62
Breast		0.26	**0.03**
Liver		0.28	0.36
Pancreas		0.40	**0.04**
Other		0.36	0.41

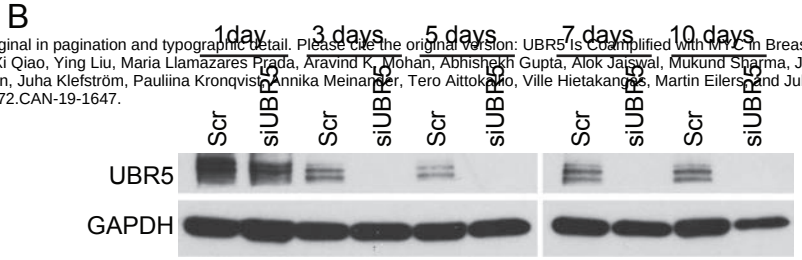

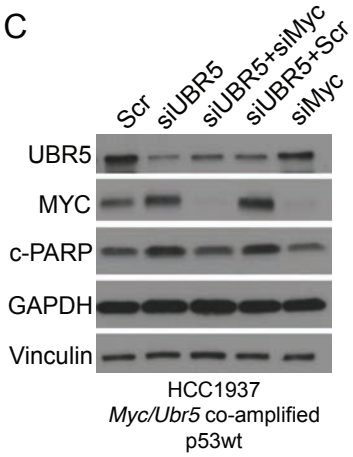

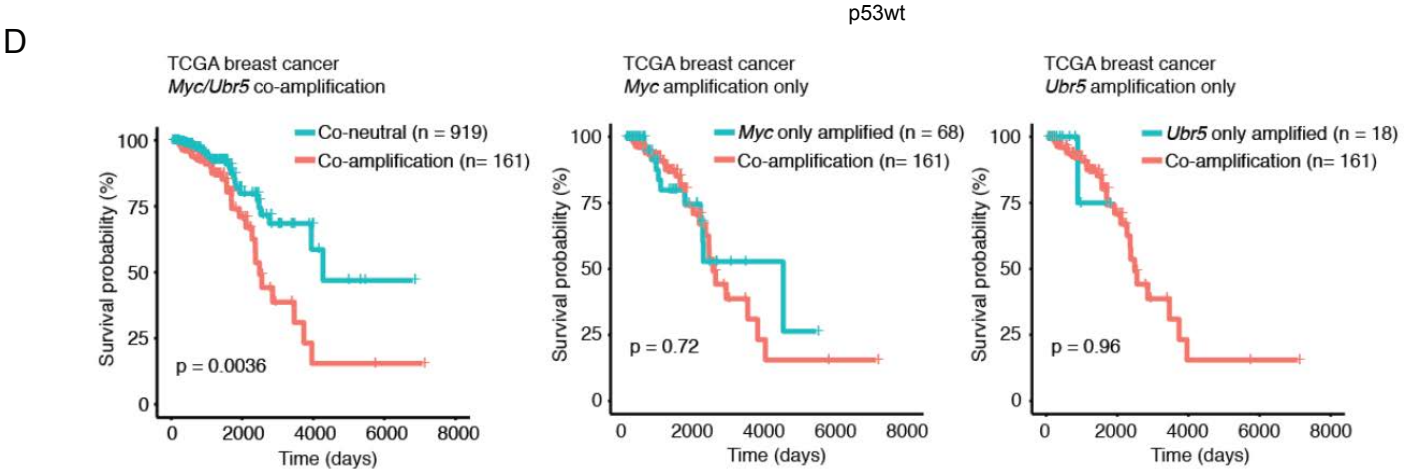

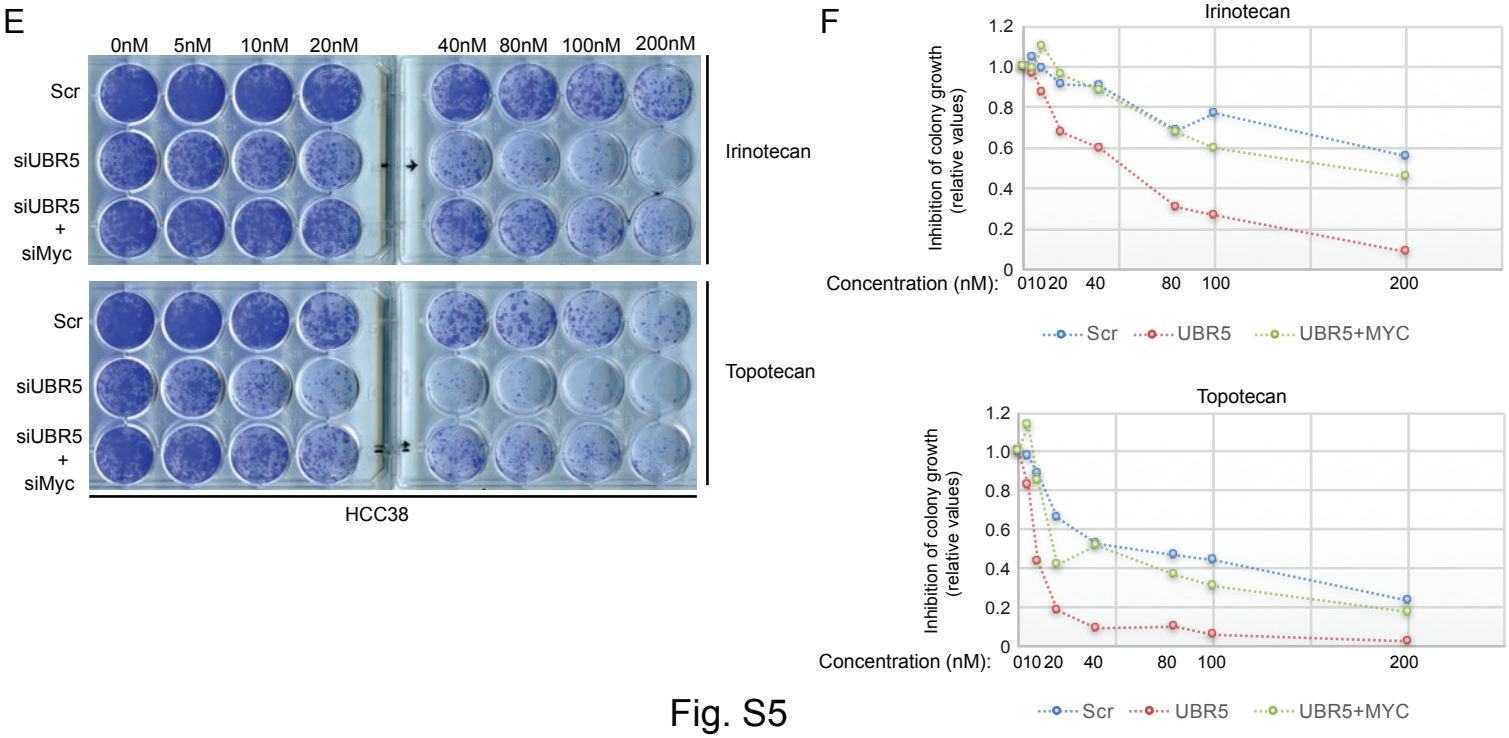

Fig. S5

Fig. S5| A) Pearson correlation for the relationship between of Myc and Ubr5 mRNA expression in cell lines from indicated tumor types. **B)** Validation of longterm inhibition of UBR5 protein expression from parallell cell cultures from those that were used for xenograft experiment shown in figure 5C. **C)** MYC-dependent PARP cleavage in UBR5 siRNA treated HCC1937 cells. **D)** Overall survival analysis of TCGA breast cancer patients that harbour different amplification status of Myc and Ubr5. **E)** Colony growth assay of siRNA transfected HCC38 cells was performed following 24 hours treatment with Irinotecan or Topotecan. **F)** Quantification of drug response fold changes relative to Scr siRNA in (E).

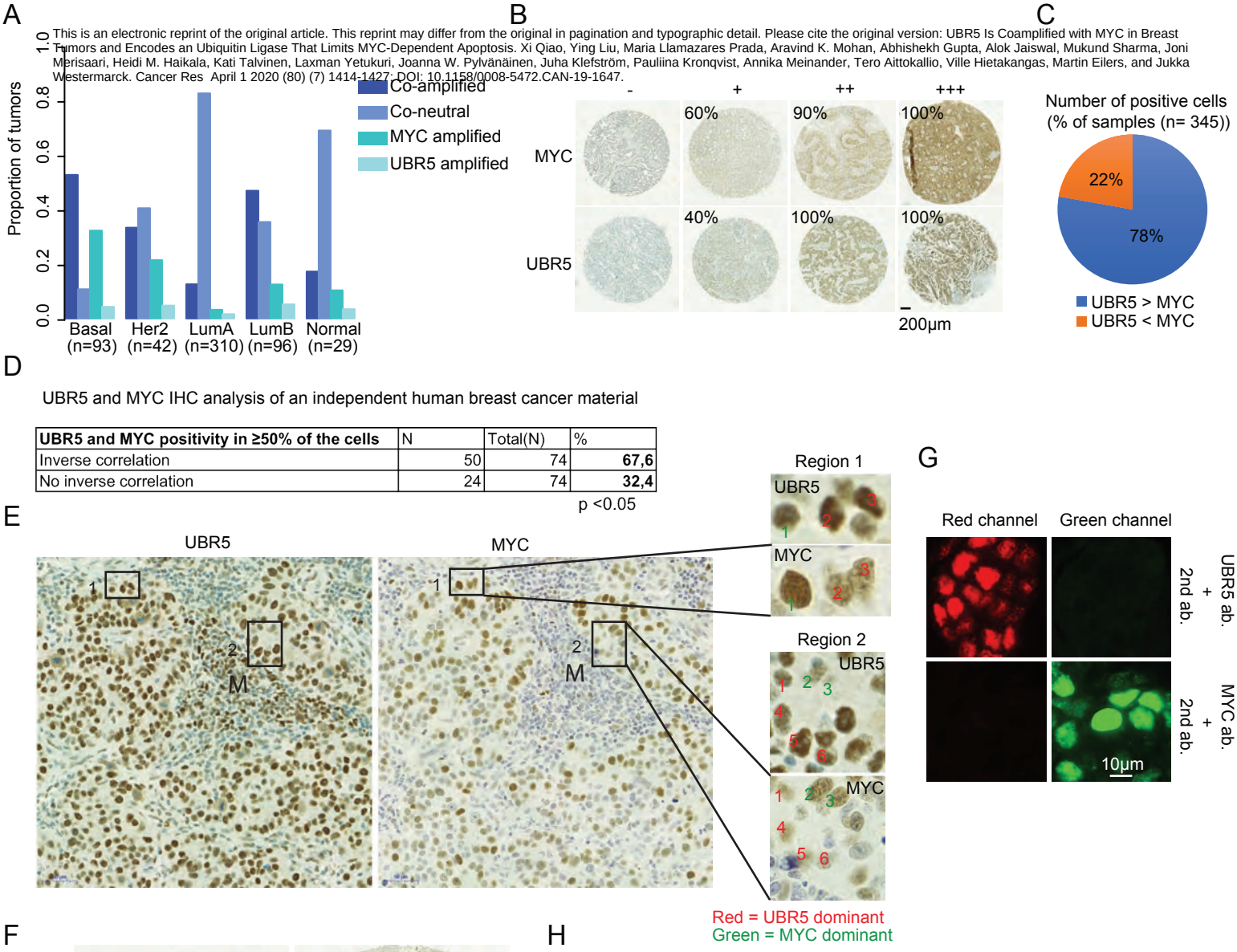

Fig. S6

Fig. S6 A) Ubr5 and Myc amplification status in different breast cancer subtypes. **B)** Immunohistochemical staining of UBR5 and MYC in human breast cancer tissues. Shown are representative examples of UBR5 and MYC intensities graded from 0 to 3+. % means percentage of positively staining cells per sample. **C)** Pie-chart distribution of 345 breast cancer samples based on whether number of tumour cells positive for either UBR5 or MYC in a tumour sample exceeded each other. **D)** Immunohistochemistry staining of UBR5 and MYC was performed in an independent set of breast cancer tissues. *, P < 0.05 by the Student t-test (n=74). **E)** Illustrative examples of inverse protein expression of UBR5 and MYC in individual basal type breast cancer cells by immunohistochemistry. M; Macrophage-like cells **F)** Full TMA IHC images to demonstrate that UBR5 and MYC is almost exclusively confined to tumor cells. **G)** Immunofluorescence background was examined by staining with only UBR5 or MYC primary antibodies in breast cancer tissues. **H)** Quantification of maximal intensity of UBR5 and MYC from dual immunofluorescent staining.